
AN APPLICATION OF D-VINE REGRESSION FOR THE IDENTIFICATION OF RISKY FLIGHTS IN RUNWAY OVERRUN

A PREPRINT

Hassan H. Alnasser
 Faculty of Mathematics
 Technical University of Munich
 h.alnasser@tum.de

Claudia Czado
 Faculty of Mathematics
 Technical University of Munich
 cczado@ma.tum.de

May 11, 2022

ABSTRACT

In aviation safety, runway overruns are of great importance because they are the most frequent type of landing accidents. Identification of factors which contribute to the occurrence of runway overruns can help mitigate the risk and prevent such accidents. Methods such as physics-based and statistical-based models were proposed in the past to estimate runway overrun probabilities. However, they are either costly or require experts' knowledge. We propose a statistical approach to quantify the risk probability of an aircraft to exceed a threshold at the speed of 80 knots given a set of influencing factors. This copula based D-vine regression approach is used because it allows for complex tail dependence and is computationally tractable. Data obtained from the Quick Access Recorder (QAR) for 711 flights are analyzed. We identify 41 flights with an estimated risk probability $> 10^{-3}$ for a chosen threshold and rank the effects of each influencing factor for these flights. Also, the complex dependency patterns between some influencing factors for the 41 flights are shown to be non symmetric. The D-vine regression approach, compared to physics-based and statistical-based approaches, has an analytical solution, is not simulation based and can be used to estimate very small or large probabilities efficiently.

Keywords Conditional probability estimation, D-vine regression, non Gaussian dependency, runway overrun, risky flight identification

1 Introduction

The International Air Transport Association (*IATA*) expects the number of air passengers to recover in 2024, exceeding the pre-COVID-19 level by 3 %. Long term forecast, also, shows a gradual increase in the number of passengers (domestically and internationally) post 2024 (*IATA*, 2022). Therefore, the need for improved safety procedures is essential. There has been an overall decrease in the number of accidents related to commercial aviation in the last 50 years, however, the consequences of such accidents can still result in losses of lives and huge economic costs. Hence, this motivates aviation companies and international aviation agencies to identify and evaluate various risks leading to such accidents. In 2006, the International Civil Aviation Organization (*ICAO*) published the first risk management guidelines (Burin, 2011; *ICAO*, 2006). Newer guidelines were published and widely accepted by air transport authorities and aviation manufacturers. However, the number of accidents did not decrease, especially for runway overrun accidents (Flight Safety Foundation, 2009). This encourages aviation safety oversight authorities to move towards a more proactive approach to identify and predict safety related trends (*ICAO*, 2013).

There is a considerable interest to mitigate the risk of runway excursions classified by *IATA*, such as undershoot, veer offs and runway overruns. Such excursions account for about 22 % of all civil aviation accidents between 1959-2019 (Zhao and Zhang, 2022). The increased danger during landing is due to multiple factors such as weather conditions (Wong et al., 2006) and decisions pilots must take while landing (Wang et al., 2014b; You et al., 2013). For instance, Jenkins and Aaron (2012) list unstabilized approach, tail or crosswind, high speed and poor use of the reverse thrust

as relevant causes for runway overruns. Other authors (Ahmed et al., 2014; Chang et al., 2016) focus on runway and weather conditions as risk contributors. For example, a large approach speed deviation and runway surface conditions were identified as contributing factors in the Fokker 100 overrun at Newman, Australia in January 2020 (Investigation, 2021).

Due to confidentiality reasons, access to flight data from accidents is limited. Valdés et al. (2011) compiled a database of air traffic accidents from official commissions and private entities to assign frequencies to factors contributing to 53 runway overruns. They identified long landing (landing far beyond the runway threshold) to be the riskiest, followed by high access approach speed. In this respect, a long distance to reach the controllable speed of 80 knots during landing is considered a precursor of runway overrun. This distance, we will refer to as distance to controllable speed hereafter, is our focus. In particular, we propose a novel statistical approach to estimate the conditional probability that the distance to controllable speed is exceeding a chosen threshold given a set of risk factor values.

Two approaches in modeling runway excursions have been discussed in the literature: one is based on the construction of a physics-based model allowing for simulation and the other is based on statistical models using appropriate flight data.

In the area of physics-based models, Drees et al. (2014) and Drees (2016) compiled a list of risk factors related to pilot operations and environmental conditions. These factors are expected to have an influence on the probability of runway overrun and are used as input values for a deterministic physical model. Based on flight dynamics, the physical model is utilized to quantify the associated runway distance to controllable speed. Also, a statistical distribution for each risk factor is estimated using operational flight data obtained from the Quick Access Recorder (*QAR*). These distributions, then, are used for the simulation of appropriate input values to the physical model. A simulation-based approach is needed since a large distance to controllable speed is often not observed in *QAR* based data. With simulated input values, the physical model can be used to generate the associated runway distance to controllable speed for each input value. Thus, to quantify the associated risk probability, one can count the number of simulations which yields a runway distance to controllable speed over a chosen critical threshold.

To reduce the number of simulations to obtain a nonzero risk probability estimate, the subset simulation approach of Au and Beck (2001) was used. Further, Drees (2016) proposed, for validation, the comparison of the observed distance to controllable speed from the *QAR* data to the physical model output. Wang et al. (2020), however, noted a shift to the left in the distribution of the distance to controllable speed compared to the observed one. This indicates a bias in the model output resulting from either the physical model or the distribution fitting error of the risk factors. Hence, Wang et al. (2020) proposed to replace the costly physical model by a faster deterministic surrogate model. The proposed model is based on polynomial chaos expansion (for details see Schöbi and Sudret (2019)) and an optimization approach. The optimization approach is used to calibrate the parameters of the fitted input distributions to the physical model to better match the *QAR* observed distribution.

Several statistical approaches have also been utilized. For example, unconditional frequency and hierarchical Bayesian models have been considered in Arnaldo Valdés et al. (2018). Gu and Wang (2014) used a linear regression model for the landing distance, while Wagner and Barker (2014) applied logistic regression and its Bayesian version. Both models were used to model the probability of fatalities using 1400 records of runway excursions happened between 1970 and 2009. The problem of hard landings, also, was considered in Hu et al. (2016) where a support vector machine model was applied. Further, discrete Bayesian networks have been utilized. Zwirgmaier and Straub (2016), for example, used first order Taylor expansions to perform the necessary discretization of a designed Bayesian network. Ayra et al. (2019) used the graphical network interface (GeNIe) software (ByesFusion, 2020) which starts with a network proposed by experts. Most recently, Zhao and Zhang (2022) developed a neural network to model the landing distance.

While the physics-based modeling approach of Drees (2016) with the calibration of the input parameters suggested by Wang et al. (2020) allows for the identification of risk conditions, both models do not allow for quantifying the effect of each risk factor having on the occurrence of runway overrun. The statistical models, while not simulation based, have other shortcomings. Those suggested by Wang et al. (2014a) and Arnaldo Valdés et al. (2018) are unconditional and, thus, cannot model the influence of several risk factors jointly. This task is achieved with the Bayesian network approaches; however, they require discretization of the continuously measured risk factors. Moreover, Bayesian network approaches are often based on networks using the subjective knowledge by experts. This suggests that there is a room to develop a flexible statistical framework to allow identification of risky flights and quantify the effect of the influencing factors. Such a framework should also be able to model dependency patterns among the variable of interest, given here by the distance to controllable speed, and the set of contributing factors, especially in the tails.

Therefore, we propose to follow a copula based approach since copulas allow to describe dependence behavior separately from marginal behavior. A copula is a multivariate distribution function with uniform marginal distributions.

To increase the range of dependence patterns in high dimensions, Joe (1996) and later Bedford and Cooke (2001) proposed using conditioning to construct multivariate copulas. This requires only the specification of bivariate copula terms which yields the vine copula class. The seminal paper of Aas et al. (2009) made this pair copula construction approach applicable. The reader can consult the books by Joe (2014) and Czado (2019) as well as the survey by Czado and Nagler (2022) for details and recent developments. The vine copula class is especially suited to model asymmetric tail dependence.

We use the D-vine (quantile) regression approach of Kraus and Czado (2017) to achieve our objective. The restriction to the subclass of D-vines allows us to express the conditional distribution function of the variable of interest given the potentially influencing factors analytically. In addition, the D-vine regression is well suited to model extreme large or small conditional probabilities, allowing for tail dependence. In this paper, we show how the D-vine regression based approach can be utilized to identify risky flights, flights having a distance to controllable speed greater than 2500 meters with estimated probability $> 10^{-3}$. Among 711 flights, we identify 41 to be risky. All flights were of the same aircraft type and landed at the same airport. Furthermore, we rank the marginal effect of each contributing factor for the risky flights. The ranking, in a descending order, is given as follows: brake duration, headwind speed, time brake started, touchdown, equivalent acceleration and approach speed deviation. In addition, we study the joint behavior for all pairs of contributing factors for the risky flights. This shows dependence among the contributing factors. We show a non-symmetric dependence between time brake started and brake duration as well as between headwind speed and equivalent acceleration.

We, further, investigate if a standard linear quantile regression approach of Koenker and Bassett (1978) and Koenker and Hallock (2001) is able to estimate such small risk probabilities. This is not the case and, even more, quantile crossing occurs in this data set.

The remainder of this paper is organized as follows. In Section 2, we provide more details on the *QAR* data used. We introduce and discuss in Section 3 the shortcomings of the linear quantile regression approach with regard to estimating conditional probabilities in the tail. Following this, we review D-vine copulas briefly and discuss the D-vine (quantile) regression approach. Estimation of critical event probabilities is then discussed and presented in Section 3. Section 4 presents results from the linear quantile and the D-vine regression. Finally, a brief discussion is given in Section 5.

2 Data description

We consider the same data set used in Drees (2016) and Wang et al. (2020). The data consists of 11 continuous variables, referred to as contributing factors, and the distance to controllable speed as the response variable. The response variable is referred to *th80* hereinafter. We list in Table 1 the contributing factors which correspond to observed and measured parameters potentially leading to runway overrun incidents. It is worth mentioning that Drees (2016) considers a runway overrun incident when a stop margin (*SM*) is less than zero. A stop margin is the difference between a landing field length (*LFL*) and a landing distance (*LD*), $SM := LFL - LD$. See Figure 1 for illustration.

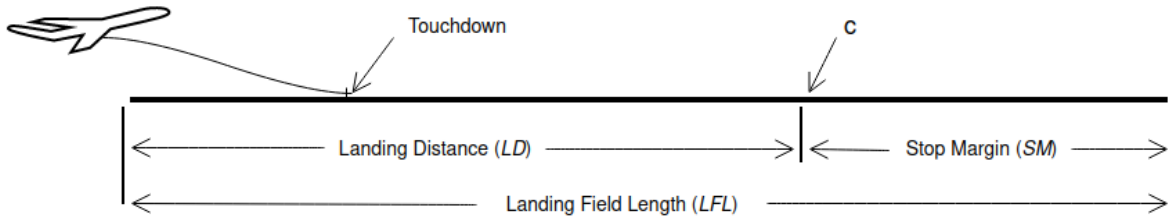


Figure 1: Landing phase illustration.

In addition, we consider the assumption that an aircraft should reach 80 knots (*kts*) ground speed before a fixed threshold *c*, leaving a reasonable *SM*. See Figure 1 for demonstration. The so-called 80 *kts* ground speed is a controllable and safe speed (Drees, 2016). More specifically, a pilot is able to control the aircraft at the speed of 80 *kts* or less. Thus, this leads to our definition of runway overrun. A runway overrun incident occurs when an aircraft exceeds the fixed threshold *c* at a speed greater than 80 *kts* without a reasonable stop margin remained.

As mentioned above, similar contributing factors have been used to assess the risk of runway overrun in Wang et al. (2020) and Drees (2016). However, they considered air density (*ad*) in place of temperature (*temp*) and reference air pressure (*refAP*). Air density was defined as $ad = refAP / (R \times temp)$ for a specific gas constant *R*. We use, in our application, the observed values of *temp* and *refAP* instead of the derived *ad*.

Table 1 Contributing factors' definitions and measurement units.

Contributing Factor	Definition
Headwind speed (<i>hws</i>)	Headwind speed measured at touchdown (<i>td</i>) in <i>m/s</i> .
Temperature (<i>temp</i>)	Temperature in <i>Kelvin</i> provided by <i>METAR</i> ¹ .
Reference air pressure (<i>refAP</i>)	Reference air pressure in <i>hPa</i> .
Approach speed deviation (<i>asd</i>)	Deviation in speed between target approach speed and the actual true airspeed at <i>td</i> in <i>m/s</i> .
Time of deploying reversers (<i>trd</i>)	Time reversers deployed after <i>td</i> in seconds <i>s</i> .
Time of deploying spoilers (<i>tsd</i>)	Time spoilers deployed after <i>td</i> in <i>s</i> .
Landing mass (<i>lm</i>)	Landing weight taken at <i>td</i> in <i>kg</i> .
Time of starting brake (<i>tbs</i>)	Time brakes started after <i>td</i> in <i>s</i> .
Duration of braking (<i>bd</i>)	Brake duration until 80 <i>kts</i> in <i>s</i> .
Touchdown Distance (<i>td</i>)	Distance from <i>th</i> to <i>td</i> in <i>m</i> .
Equivalent acceleration (<i>ea</i>)	Constant deceleration from <i>td</i> to 80 <i>kts</i> in <i>m/s</i> ² .

To insure comparability, we focus on 711 flights of the same aircraft type. All 711 flights landed on the same runway in both directions. Moreover, there are additional discrete factors which we do not include because they have the same setting (or value) for the 711 flights. These factors describe aircraft systems which are implemented when an aircraft is either landing or taking off. Such factors have several configurations. See Table 2 for more details. For example, the combination of fully extended flaps and slats generates more drag (see Figure 2) and is used to fly slower at a higher power setting (Sforza, 2014). We shade in Table 2 the configurations and weather condition we observed in our flight data.

Table 2 Aircraft systems and their configurations as well as runway condition.

flapConfig ² :	CONF 0°	CONF 10°	CONF 20°	CONF 25°	CONF 30°
slatConfig ³ :	CONF 0°	CONF 5°	CONF 10°	CONF 20°	
revThrust ⁴ :	3/ALL OUT	FullRev	2 OUT		
splrSysStat ⁵ :	OP	≤ 2 FAULT	≤ 4 FAULT	5/ALL FAULT	
brkSysStat ⁶ :	OP	DEGRADED	INOP		
rwYCond ⁷ :	DRY	WET	VICINITY		

3 Methodology

We propose a statistical model to estimate risk probabilities for our flight data. The estimated risk probabilities correspond to a flight exceeding a chosen threshold *c* at the controllable speed of 80 *kts*. However, we first introduce some notations and terminologies, which will help us in defining our model. We, then, review linear quantile regression (*lqr*), our a benchmark model, and discuss some of its disadvantages.

¹METEorological Aerodrome Report

²Flap configuration position at different degrees.

³Slat configuration position at different degrees.

⁴Reverse thrust either applied fully or partially.

⁵Spoiler system status either operative or partially/fully inoperative.

⁶Brake system status (operative, degraded, inoperative).

⁷Runway condition.

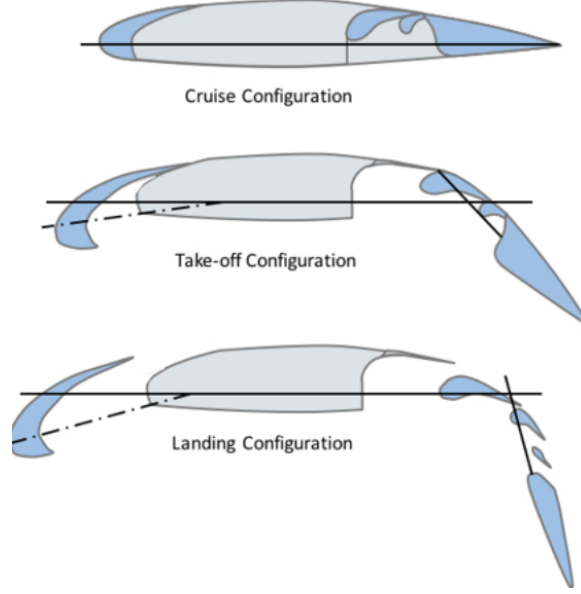


Figure 2: Three different flight phases (cruise, take-off and landing) with different flap and slat configurations (Simons, 2015).

Data terminology

Suppose we have observed data $\mathbf{y} = (y_1, \dots, y_n)^\top$ composed of n independent observations. Each observation y_i ($i = 1, \dots, n$) has d covariates collected in the covariate vector \mathbf{x}_i such that $\mathbf{x}_i = (x_{i1}, \dots, x_{id})^\top$.

3.1 Linear quantile regression

When it comes to methods to predict conditional quantiles, the literature is rich with such methods. The first and probably the most widely used is the *lqr* (Koenker and Hallock, 2001; Koenker and Bassett, 1978). Further methods followed after such as local quantile regression (Spokoiny et al., 2013), semiparametric quantile regression (Noh et al., 2015) and nonparametric quantile regression (Li et al., 2013). While most of the recent extensions to *lqr* are nonparametric (Koenker et al., 2017), we use the parametric *lqr* of Koenker (2005). This is due to the linear relationship between *th80* and the contributing factors. See Figure 11 in Appendix B for illustration.

Koenker and Bassett (1978) introduced the parametric *lqr* as a method to estimate conditional quantiles of a response variable Y given d covariates, $\mathbf{x} = (x_1, \dots, x_d)^\top$. More specifically, the conditional quantile function is defined as:

$$q_\alpha^{(l)}(x_1, \dots, x_d) := F_{Y|\mathbf{X}}^{-1}(\alpha | x_1, \dots, x_d), \quad (1)$$

where $F_{Y|\mathbf{X}}$ is the conditional distribution function of Y given $\mathbf{X} = \mathbf{x}$ and $\alpha \in (0, 1)$ is the quantile level. It is important to note that the *lqr* estimator is more robust in the presence of non-normal errors and outliers (Hao and Naiman, 2007). In addition, the *lqr* gives a more complete representation of the conditional response distribution for a set of α levels.

Originally, Koenker and Bassett (1978) assumed a linear model for the conditional quantile function given by

$$q_\alpha^{(l)}(x_{i1}, \dots, x_{id}) = \beta_0 + \sum_{j=1}^d \beta_j x_{ij}, \quad (2)$$

where $\beta \in \mathbb{R}^{d+1}$ represents the unknown regression coefficients. These coefficients are estimated by solving the minimization problem:

$$\min_{\beta \in \mathbb{R}^{d+1}} \left\{ \alpha \sum_{i=1}^n \left(y_i - \beta_0 - \sum_{j=1}^d \beta_j x_{ij} \right) + (1 - \alpha) \sum_{i=1}^n \left(\beta_0 + \sum_{j=1}^d \beta_j x_{ij} - y_i \right) \right\}. \quad (3)$$

Although *lqr* is a useful approach without any distributional assumptions, it has a major flaw in that the regression lines of several quantile levels may cross. Figure 3 shows four fitted quantile regression lines crossing using the observed *QAR* data. The cause of this is the piecewise linear formulation of the check function in (3). Bernard and Czado (2015), additionally, show that Equation (2) is only satisfied when the dependent variable and covariates (Y, \mathbf{X}) are jointly multivariate normally distributed.

In the next subsections, we introduce the concept of D-vine copulas and D-vine copula based quantile regression. The D-vine regression approach overcomes the mentioned pitfalls of the *lqr*.

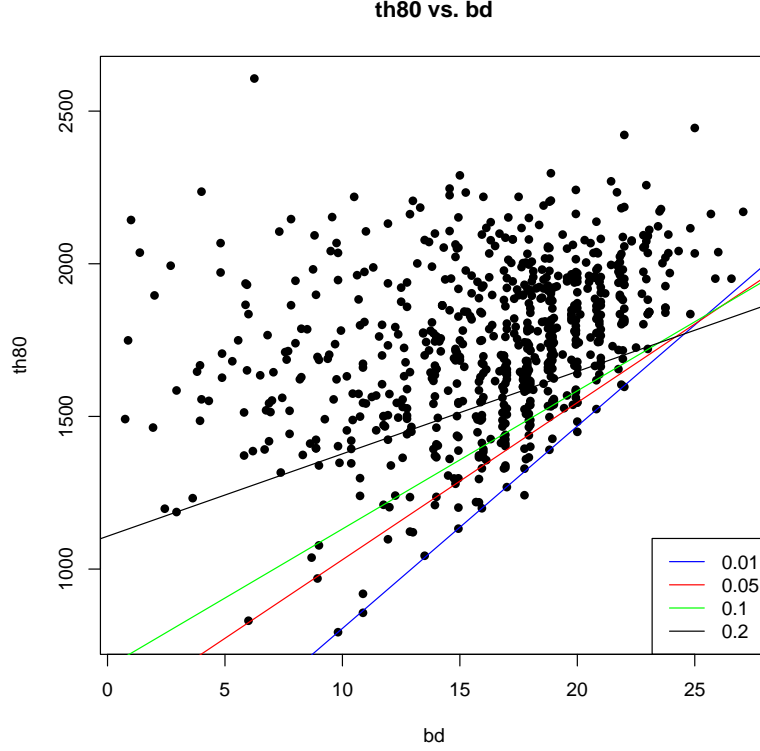


Figure 3: Fitted quantile regression lines for *th80* vs. *bd* at $\alpha = (0.01, 0.05, 0.1, 0.2)^\top$.

3.2 D-vine copulas

Modeling the dependence structure of multivariate data is an important step in predictive modeling. Copulas have been used successfully in modeling complex dependence structures in multiple disciplines, such as geotechnical engineering (Tang et al., 2015) and financial time series (Patton, 2012).

A d -dimensional copula C is a d -variate distribution function defined on the unit hypercube $[0, 1]^d$ with uniformly distributed margins. Sklar (1959) showed that for every multivariate random vector $\mathbf{X} = (X_1, \dots, X_d)^\top$ with joint distribution function F and marginal distribution functions F_1, \dots, F_d , there exists a copula C , such that

$$F(x_1, \dots, x_d) = C(F_1(x_1), \dots, F_d(x_d)), \quad (4)$$

for $\mathbf{x} \in \mathbb{R}^d$. The copula C is unique when \mathbf{X} is absolutely continuous. An advantage of the copula approach is that it allows for separation of the marginal behavior of each variable from the joint dependence structure specified by the copula C . This is different from the standard approach, *i.e.* multivariate normal, where all margins and the joint distribution are assumed normal and, thus, only allow for symmetric dependence.

To obtain uniformly distributed margins, $U_j := F_j(X_j)$, we apply the Probability Integral Transform (*PIT*), $F_j(\cdot)$, to each variable X_j , $j = 1, \dots, d$. Consequently, this allows us to write the joint density function f of Equation (4) as a product of the copula density c and the marginal densities as

$$f(x_1, \dots, x_d) = c(F_1(X_1), \dots, F_d(X_d)) \cdot f_1(x_1) \dots f_d(x_d). \quad (5)$$

Note that the copula approach permits us to specify arbitrary margins. X_j can, for example, be Gamma or Beta distributed. The choice of multivariate copula families was limited with regard to the allowable degree of asymmetric tail dependence in the past. To increase the modeling flexibility, Joe (1996) constructed multivariate copulas from bivariate copulas. The idea of conditioning was utilized to build a valid multivariate copula distribution using the bivariate copulas. Since there are multiple ways to select the needed conditioning variables, Bedford and Cooke (2001) proposed a graphical structure called a vine tree structure to identify the different choices for the conditioning variables. This led to the birth of the regular (R)-vine copula class, which is the topic of recent books (Czado (2019); Joe (2014)).

The regular vine tree structure consists of a set of linked trees (T_1, \dots, T_{d-1}) where the nodes in the first tree T_1 are the variables X_1, \dots, X_d . The edges from T_1 will become the nodes of T_2 , and any edge of tree T_2 is allowed as long as the nodes of T_2 share a node in T_1 . This tree construction principle is carried forward for the remaining trees and is called the proximity condition. Now, each edge of a tree is associated with a bivariate pair copula. The product of all these pair copula densities, which are evaluated at conditional distribution functions, is then a valid joint copula density. The modeling potential, including step-wise estimation approaches, was first discussed in Aas et al. (2009). This is also where the term Pair Copula Construction (*PCC*) for constructing vine copulas was used.

An earlier review on the use of *PCC* in financial applications was given in Aas (2016), and in Chapter 11 of Czado (2019) further applications in the engineering and life sciences domains were presented. More recently, Czado and Nagler (2022) gives an overview of vine copula based modeling.

Two popular sub-classes of regular vines are the canonical (C)-vines and drawable (D)-vines. For our conditional risk assessment approach, we will use D-vines. The D-vine quantile regression, first proposed by Kraus and Czado (2017), models the dependence between the response and covariates flexibly and also allows for a forward variable selection. These attributes make the D-vine approach suitable for our application since we want to model the distance to controllable speed conditioned on a set of risk factors flexibly.

The following notations are needed to describe the conditional distributions in the D-vine class. For a d -dimensional random vector \mathbf{X} , let a set $\mathcal{D} \subset \{1, \dots, d\}$ such that $\mathbf{X}_{\mathcal{D}}$ is a sub random vector and $\mathbf{x}_{\mathcal{D}}$ is its value. For $i, j \in \{1, \dots, d\} \setminus \mathcal{D}$, we define:

- $C_{X_i, X_j; \mathbf{X}_{\mathcal{D}}}(\cdot, \cdot; \mathbf{x}_{\mathcal{D}})$ is the bivariate copula associated with the conditional distribution of (X_i, X_j) given $\mathbf{X}_{\mathcal{D}} = \mathbf{x}_{\mathcal{D}}$. We use the following abbreviation $C_{ij; \mathcal{D}}(\cdot, \cdot; \mathbf{x}_{\mathcal{D}})$ and $c_{ij; \mathcal{D}}(\cdot, \cdot; \mathbf{x}_{\mathcal{D}})$ for the distribution function and density, respectively.
- $F_{X_i | \mathbf{X}_{\mathcal{D}}}(\cdot | \mathbf{x}_{\mathcal{D}})$ is the univariate conditional distribution of the random variable X_i given $\mathbf{X}_{\mathcal{D}} = \mathbf{x}_{\mathcal{D}}$, which is abbreviated by $F_{i | \mathcal{D}}(\cdot | \mathbf{x}_{\mathcal{D}})$.
- $C_{U_i | \mathbf{U}_{\mathcal{D}}}(\cdot | \mathbf{u}_{\mathcal{D}})$ is the conditional distribution of the *PIT* random variable U_i given $\mathbf{U}_{\mathcal{D}} = \mathbf{u}_{\mathcal{D}}$, which is abbreviated by $C_{i | \mathcal{D}}(\cdot | \mathbf{u}_{\mathcal{D}})$.

Czado (2010) expresses the joint density f in the case of a D-vine distribution as:

$$f(x_1, \dots, x_d) = \prod_{k=1}^d f_k(x_k) \prod_{i=1}^{d-1} \prod_{j=i+1}^d c_{ij; i+1, \dots, j-1}(F_{i | i+1, \dots, j-1}(x_i | x_{i+1}, \dots, x_{j-1}), F_{j | i+1, \dots, j-1}(x_j | x_{i+1}, \dots, x_{j-1}); x_{i+1}, \dots, x_{j-1}), \quad (6)$$

for distinct indices i and j , $i < j$.

An illustration of a four-dimensional D-vine distribution is given in Example 1, and its graphical representation is shown in Figure 4.

Example 1 (Four-dimensional D-vine). A D-vine distribution for $d = 4$ has a joint density given by

$$\begin{aligned} f(x_1, x_2, x_3, x_4) &= f_4(x_4) f_3(x_3) f_2(x_2) f_1(x_1) \\ &\quad c_{12}(F_1(x_1), F_2(x_2)) \cdot c_{23}(F_2(x_2), F_3(x_3)) \cdot c_{34}(F_3(x_3), F_4(x_4)) \quad (T_1) \\ &\quad c_{13;2}(F_{1|2}(x_1|x_2), F_{3|2}(x_3|x_2)) \cdot c_{24;3}(F_{2|3}(x_2|x_3), F_{4|3}(x_4|x_3)) \quad (T_2) \\ &\quad c_{14;23}(F_{1|23}(x_1|x_2, x_3), F_{4|23}(x_4|x_2, x_3)). \quad (T_3) \end{aligned}$$

$f(x_1, x_2, x_3, x_4)$ is decomposed into

$$f_{4|123}(x_4|x_1, x_2, x_3) \cdot f_{3|12}(x_3|x_1, x_2) \cdot f_{2|1}(x_2|x_1) \cdot f_1(x_1),$$

where each conditional density is considered separately. We write $f_{3|12}(x_3|x_1, x_2)$ in terms of bivariate copulas and a marginal density using Sklar's theorem (4) as follows:

$$\begin{aligned} f_{3|12}(x_3|x_1, x_2) &= \frac{f_{13|2}(x_1, x_3|x_2)}{f_{1|2}(x_1|x_2)} \\ &= \frac{c_{13;2}(F_{1|2}(x_1|x_2), F_{3|2}(x_3|x_2)) \cdot f_{1|2}(x_1|x_2) \cdot f_{3|2}(x_3|x_2)}{f_{1|2}(x_1|x_2)} \\ &= c_{13;2}(F_{1|2}(x_1|x_2), F_{3|2}(x_3|x_2)) \cdot f_{3|2}(x_3|x_2), \end{aligned} \quad (7)$$

where, further, we decompose $f_{3|2}(x_3|x_2)$ into

$$\begin{aligned} f_{3|2}(x_3|x_2) &= \frac{f_{23}(x_2, x_3)}{f_2(x_2)} \\ &= \frac{c_{23}(F_2(x_2), F_3(x_3)) \cdot f_2(x_2) \cdot f_3(x_3)}{f_2(x_2)} \\ &= c_{23}(F_2(x_2), F_3(x_3)) \cdot f_3(x_3). \end{aligned}$$

Similarly, we write $f_{4|123}(x_4|x_1, x_2, x_3)$ as

$$\begin{aligned} f_{4|123}(x_4|x_1, x_2, x_3) &= c_{14;23}(F_{1|23}(x_1|x_2, x_3), F_{4|23}(x_4|x_2, x_3)) \\ &\quad \cdot c_{24;3}(F_{2|3}(x_2|x_3), F_{4|3}(x_4|x_3)) \cdot c_{34}(F_3(x_3), F_4(x_4)) \cdot f_4(x_4). \end{aligned}$$

This gives us the joint density given above in Example 1, and the corresponding D-vine tree structure is given in Figure 4. We see the variables are the nodes of tree T_1 , and the edges of tree T_1 correspond to the non conditional bivariate copula densities in Example 1. The arrangement of the variables in tree T_1 is arbitrary, so we denote this specific order by $X_1 - X_2 - X_3 - X_4$. The edges 12, 23 and 34 now become nodes in tree T_2 . The nodes 12 and 23 can be connected by an edge denoted by 13;2 since the edges 12 and 23 share the common node 2 in tree T_1 .

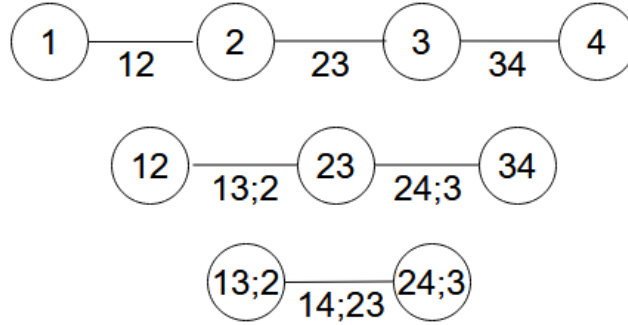


Figure 4: Graphical representation of a four-dimensional D-vine with order $X_1 - X_2 - X_3 - X_4$.

To fit a D-vine copula with a specific order to given data, the pair copulas in Equation (6) will be estimated parametrically for our application. This allows for easy model simulation. In addition, we assume the copulas associated with the conditional distributions $C_{i,j;\mathcal{D}}$ do not depend on the specific value $\mathbf{x}_{\mathcal{D}}$ of the conditioning vector $\mathbf{X}_{\mathcal{D}}$. This assumption is called the simplifying assumption, and it is assumed in (6) for tractability reasons.

To evaluate the conditional distributions $F_{i|i+1,\dots,j-1}(x_i|x_{i+1}, \dots, x_{j-1})$ in Equation (6), we only need pair copulas specified in the lower trees of the D-vine. Together with the simplifying assumption, this allows us to determine them recursively (Joe, 1996). In detail, let $\mathcal{D} = \{i+1, \dots, j-1\}$, then we can write $F_{i|i+1,\dots,j-1}(x_i|x_{i+1}, \dots, x_{j-1})$ as $F_{i|\mathcal{D}}(x_i|\mathbf{x}_{\mathcal{D}})$. Subsequently, we can express $F_{i|\mathcal{D}}(x_i|\mathbf{x}_{\mathcal{D}})$ for $l \in \mathcal{D}$ and $\mathcal{D}_{-l} := \mathcal{D} \setminus \{l\}$ as

$$F_{i|\mathcal{D}}(x_i|\mathbf{x}_{\mathcal{D}}) = h_{i|l;\mathcal{D}_{-l}}(F_{i|\mathcal{D}_{-l}}(x_i|\mathbf{x}_{\mathcal{D}_{-l}}) | F_{l|\mathcal{D}_{-l}}(x_l|\mathbf{x}_{\mathcal{D}_{-l}})), \quad (8)$$

where for $i, j \notin \mathcal{D}, i < j$, $h_{i|j;\mathcal{D}}(u|v) := \partial C_{ij;\mathcal{D}}(u, v) / \partial v = C_{i|j;\mathcal{D}}(u|v)$ and, similarly, $h_{j|i;\mathcal{D}}(v|u) = \partial C_{ij;\mathcal{D}}(u, v) / \partial u = C_{j|i;\mathcal{D}}(v|u)$. These are called h -functions, which are associated with the pair-copula $C_{ij;\mathcal{D}}$.

Note that the h -functions are independent of the specific value \mathbf{x}_D for \mathbf{X}_D because of the simplifying assumption. A general property of vine densities is that all required conditional distribution functions can be determined using only h -functions.

Example 2 (Conditional distribution functions). We illustrate how to determine conditional distribution functions for a three-dimensional vector $\mathbf{X} = (X_1, X_2, X_3)^\top$:

$$\begin{aligned}
F_{3|12}(x_3|x_1, x_2) &= \int_{-\infty}^{x_3} f_{3|12}(t_3|x_1, x_2) dt_3 \\
&= \int_{-\infty}^{x_3} c_{13;2}(F_{1|2}(x_1|x_2), F_{3|2}(t_3|x_2)) \cdot f_{3|2}(t_3|x_2) dt_3 \\
&= \int_{-\infty}^{x_3} \frac{\partial}{\partial F_{1|2}(x_1|x_2)} \frac{\partial}{\partial F_{3|2}(t_3|x_2)} C_{13;2}(F_{1|2}(x_1|x_2), F_{3|2}(t_3|x_2)) \\
&\quad \cdot f_{3|2}(t_3|x_2) dt_3 \\
&= \frac{\partial}{\partial F_{1|2}(x_1|x_2)} \int_{-\infty}^{x_3} \left[\frac{\partial}{\partial t_3} C_{13;2}(F_{1|2}(x_1|x_2), F_{3|2}(t_3|x_2)) \right] dt_3 \\
&= \frac{\partial}{\partial F_{1|2}(x_1|x_2)} C_{13;2}(F_{1|2}(x_1|x_2), F_{3|2}(x_3|x_2)) \\
&= h_{1|3;2}(h_{1|2}(x_1|x_2)|h_{3|2}(x_3|x_2)).
\end{aligned}$$

3.3 D-vine copula based quantile regression

The D-vine copula based quantile regression, proposed by Kraus and Czado (2017), predicts the quantile of a response variable Y given some covariates X_1, \dots, X_d , for $d \geq 1$. For convenience, we use the following notation: $Y \sim F_Y$, and $X_j \sim F_j$, $j = 1, \dots, d$. This helps us in defining the conditional quantile function $Y|\mathbf{X} = \mathbf{x}$ for level $\alpha \in (0, 1)$, which is expressed as the inverse of the conditional distribution function of $Y|\mathbf{X}$:

$$q_\alpha(x_1, \dots, x_d) := F_{Y|X_1, \dots, X_d}^{-1}(\alpha|x_1, \dots, x_d). \quad (9)$$

Applying the *PIT* to the response Y and to the covariates X_1, \dots, X_d , we obtain $V := F_Y(Y)$ and $U_j := F_j(X_j)$, respectively. With the corresponding observed *PIT* values $v := F_Y(y)$ and $u_j := F_j(x_j)$, we have the following:

$$\begin{aligned}
F_{Y|X_1, \dots, X_d}(y|x_1, \dots, x_d) &= P(Y \leq y | X_1 = x_1, \dots, X_d = x_d) \\
&= P(F_Y(Y) \leq v | F_1(X_1) = u_1, \dots, F_d(X_d) = u_d) \\
&= C_{V|U_1, \dots, U_d}(v|u_1, \dots, u_d) \\
&= C_{V|U_1, \dots, U_d}(F_Y(y)|F_1(x_1), \dots, F_d(x_d)).
\end{aligned} \quad (10)$$

Equation (10), thus, allows us to express Equation (9) as:

$$F_{Y|X_1, \dots, X_d}^{-1}(\alpha|x_1, \dots, x_d) = F_Y^{-1} \left(C_{V|U_1, \dots, U_d}^{-1}(\alpha|F_1(x_1), \dots, F_d(x_d)) \right). \quad (11)$$

This implies that the conditional quantile function can be expressed as the inverse of both the marginal distribution function of the response and the conditional copula quantile function given the observed *PIT* value of \mathbf{x} . Hence, we obtain an estimate of the conditional quantile function as:

$$\hat{q}_\alpha(x_1, \dots, x_d) := \hat{F}_Y^{-1} \left(\hat{C}_{V|U_1, \dots, U_d}^{-1}(\alpha|\hat{u}_1, \dots, \hat{u}_d) \right), \quad (12)$$

where $\hat{u}_j := \hat{F}_j(x_j)$ is the estimated *PIT* value of x_j , $j = 1, \dots, d$, and $\hat{C}_{V|U_1, \dots, U_d}^{-1}$ is an estimate of the conditional quantile function for V given U_1, \dots, U_d .

We now specify a D-vine copula to $(V, U_1, \dots, U_d)^\top$ such that V is fixed as the first node in the first tree. The order of the D-vine is $V-U_{k_1}-\dots-U_{k_d}$, where $(k_1, \dots, k_d)^\top$ is allowed to be an arbitrary permutation for $(1, \dots, d)^\top$. This allows for flexibility because the order of the U_j is chosen to maximize the conditional likelihood (Kraus and Czado, 2017). Note that since we expressed $C_{V|U_1, \dots, U_d}(v|u_1, \dots, u_d)$ in terms of nested h -functions in Equation (8), we can express the conditional quantile function in terms of inverse h -functions.

It is important to mention that $C_{V|U_1, \dots, U_d}^{-1}(\alpha|u_1, \dots, u_d)$ is monotonically increasing in α , meaning that crossing of quantile functions is not possible. As a result, the D-vine copula based quantile regression overcomes the pitfall of the benchmark *lqr*.

3.4 Estimation of D-vine quantile regression

To estimate the conditional quantile function in Equation (12) utilizing Equation (11), we need to estimate the marginal distribution functions of all variables, including the response, and the conditional copula distribution. We proceed in a two step approach. First, we estimate the required marginal distribution functions and, secondly, estimate the h -functions based on the pair copulas.

Marginal distribution function estimation

In order to fit marginal distributions to our variables, we utilize parametric and a mixture of parametric univariate distributions. Fitting univariate parametric distributions to continuous data is a standard task in statistics. However, choosing an appropriate probability distribution for the univariate random variable needs a careful examination. We use maximum likelihood (ML) estimation to estimate the parameters of the chosen distribution.

Sometimes standard univariate parametric distributions do not fit the data at hand. A mixture of univariate parametric distributions enhances modeling flexibility considerably. Here we focus on a mixture of univariate normal distributions, which we express as a weighted sum of S normal distributions $\{\psi_1(x; \Theta_1), \dots, \psi_S(x; \Theta_S)\}$. The weights $\{\omega_1, \dots, \omega_S\}$ sum to one and each distribution has its own parameters Θ . We express this as

$$\text{minimize} \quad f(x; \Theta_1, \dots, \Theta_S) = \sum_{s=1}^S \omega_s \psi_s(x; \Theta_s), \quad \text{subject to} \quad \sum_{s=1}^S \omega_s = 1, \quad (13)$$

where each normal distribution with density $\psi_s(x; \Theta_s)$ has its own parameters, $\Theta_s = (\mu_s, \sigma_s)^\top$, $s = 1, \dots, S$. The distribution parameters are estimated using an expectation-maximization (EM) algorithm. The algorithm maximizes the conditional expected (complete-data) log likelihood at each M-step (McLachlan and Peel, 2000).

After obtaining the estimated marginal distribution functions, \hat{F}_Y and \hat{F}_j , $j = 1, \dots, d$, we transform the observed data to pseudo copula data $\hat{v}_i := \hat{F}_Y(y_i)$ and $\hat{u}_{ij} := \hat{F}_j(x_{ij})$, $j = 1, \dots, d$, $i = 1, \dots, n$. Let $\hat{\mathbf{u}}_i = (\hat{u}_{i1}, \dots, \hat{u}_{id})^\top$ for $i = 1, \dots, n$, then $\{(\hat{v}_i, \hat{\mathbf{u}}_i) : i = 1, \dots, n\}$ is an approximate independent and identically distributed (i.i.d.) sample of the PIT random vector $(V, U_1, \dots, U_d)^\top$.

3.4.1 Parametric D-vine copula estimation

In Equation (12), we fit a D-vine with order $V - U_{k_1} - \dots - U_{k_d}$ to pseudo copula data. The ordering $\mathbf{k} = (k_1, \dots, k_d)^\top$ of the variables is chosen in a stepwise fashion to maximize the conditional log-likelihood (cll) of the fitted D-vine. We define the cll of an estimated D-vine with ordering \mathbf{k} , fitted parametric pair-copula families $\hat{\mathcal{F}}$ and corresponding copula parameters $\hat{\theta}$ as follows for given pseudo copula data $(\hat{\mathbf{v}} = (\hat{v}_1, \dots, \hat{v}_2)^\top, \hat{\mathcal{U}} = \{\hat{\mathbf{u}}_i, i = 1, \dots, n\})$:

$$cll(\mathbf{k}, \hat{\mathcal{F}}, \hat{\theta}; \hat{\mathbf{v}}, \hat{\mathcal{U}}) := \sum_{i=1}^n \log c_{V|U}(\hat{v}_i | \hat{\mathbf{u}}_i; \mathbf{k}, \hat{\mathcal{F}}, \hat{\theta}), \quad (14)$$

where the conditional copula density $c_{V|U}$ is expressed as:

$$\begin{aligned} c_{V|U}(\hat{v}_i | \hat{\mathbf{u}}_i; \mathbf{k}, \hat{\mathcal{F}}, \hat{\theta}) &= c_{VU_{k_1}}(\hat{v}_i, \hat{u}_{ik_1}; \hat{\mathcal{F}}_{VU_{k_1}}, \hat{\theta}_{VU_{k_1}}) \times \\ &\prod_{j=2}^d c_{VU_{k_j}; U_{k_1}, \dots, U_{k_{j-1}}}(\hat{C}_{V|U_{k_1}, \dots, U_{k_{j-1}}}(\hat{v}_i | \hat{u}_{ik_1}, \dots, \hat{u}_{ik_{j-1}}), \\ &\quad \hat{C}_{U_{k_j}|U_{k_1}, \dots, U_{k_{j-1}}}(\hat{u}_{ik_j} | \hat{u}_{ik_1}, \dots, \hat{u}_{ik_{j-1}}); \hat{\mathcal{F}}_{VU_{k_j}; U_{k_1}, \dots, U_{k_{j-1}}}, \hat{\theta}_{VU_{k_j}; U_{k_1}, \dots, U_{k_{j-1}}}). \end{aligned}$$

Here $\hat{\mathcal{F}}_{VU_{k_j}; U_{k_1}, \dots, U_{k_{j-1}}}$ and $\hat{\theta}_{VU_{k_j}; U_{k_1}, \dots, U_{k_{j-1}}}$ denote the fitted pair copula family and its copula parameter estimate of $C_{VU_{k_j}; U_{k_1}, \dots, U_{k_{j-1}}}$, respectively. Kraus and Czado (2017) provide more details on the D-vine regression forward selection algorithm. The algorithm sequentially constructs a D-vine while maximizing the model's cll in each step and stops when the model's conditional log-likelihood can not be improved. This results in parsimonious models where only influential covariates are included. To account for model complexity, two standard selection criteria, which includes the number of needed parameters in the D-vine regression, are considered: AIC-corrected conditional log-likelihood (ccl^{AIC}) and BIC-corrected conditional log-likelihood (ccl^{BIC}). The ccl^{AIC} is defined as:

$$ccl^{AIC}(\mathbf{k}, \hat{\mathcal{F}}, \hat{\theta}; \hat{\mathbf{v}}, \hat{\mathcal{U}}) := -2ccl(\mathbf{k}, \hat{\mathcal{F}}, \hat{\theta}; \hat{\mathbf{v}}, \hat{\mathcal{U}}) + 2|\hat{\theta}|, \quad (15)$$

and the cll^{BIC} is defined as

$$cll^{BIC}(\mathbf{k}, \hat{\mathcal{F}}, \hat{\boldsymbol{\theta}}; \hat{\mathbf{v}}, \hat{\mathbf{U}}) := -2cll(\mathbf{k}, \hat{\mathcal{F}}, \hat{\boldsymbol{\theta}}; \hat{\mathbf{v}}, \hat{\mathbf{U}}) + \log(n)|\hat{\boldsymbol{\theta}}|. \quad (16)$$

Kraus and Czado (2017) state that the AIC-corrected cll^{AIC} is sufficient since only up to two parameters per copula family are estimated. Example 3 illustrates the forward selection algorithm on a four-dimensional vector $(Y, X_1, X_2, X_3)^\top$.

Example 3 (Forward selection algorithm on four-dimensional vector). Suppose we have a four-dimensional vector $(Y, X_1, X_2, X_3)^\top$, where Y denotes the response variable and $(X_1, X_2, X_3)^\top$ are the covariates. After transforming the data to pseudo copula data $(\hat{v}_i, \hat{u}_{i1}, \hat{u}_{i2}, \hat{u}_{i3})^\top$ for $i = 1, \dots, n$, we choose the pair $(V, U_j)^\top$, $j = 1, 2, 3$, which has the largest cll among the D-vines $V - U_j$, $j = 1, 2, 3$. Assume the pair $(V, U_3)^\top$ has the largest conditional log-likelihood, then we have two remaining variables: U_1 and U_2 . We investigate if adding U_1 or U_2 would improve the cll of the model. Assuming that adding U_1 is better than adding U_2 and if it also improves over $V - U_3$, then we update the D-vine to $V - U_3 - U_1$ from $V - U_3$. Next, we study if adding the remaining variable U_2 would improve the conditional log-likelihood of $V - U_3 - U_1$ or not. If, for example, the model's cll with order $V - U_3 - U_1$ is equal to the model's cll with order $V - U_3 - U_1 - U_2$, the algorithm returns the D-vine with order $V - U_3 - U_1$.

3.5 Estimation of critical event probabilities using the D-vine regression approach

For risk assessment, we are interested in estimating the probability of a critical event $Y > c$ for a fixed c under the conditions $\mathbf{X} = \mathbf{x}$, *i.e.*

$$\begin{aligned} \alpha_c(\mathbf{x}) &:= P(Y > c | \mathbf{X} = \mathbf{x}) = 1 - P(Y \leq c | \mathbf{X} = \mathbf{x}) \\ &= 1 - F_{Y|X_1, \dots, X_d}(c | x_1, \dots, x_d). \end{aligned} \quad (17)$$

In view of Equation (1) and Equation (12), we see $\alpha_c(\mathbf{x})$ is a function of the inverse of $q_\alpha(\mathbf{x})$ with respect to α . The conditional distribution function in Equation (17) can be estimated using a bisection algorithm to invert the conditional quantile function in the *lqr* case. However, Equation (17) is obtained directly via the Rosenblatt transform (Rosenblatt, 1952) in the case for D-vine copula based approach.

The bisection algorithm is a root-finding algorithm applied to the function with respect to α in Equation (1). The algorithm selects a sub-interval in which the root must lie in, and the sub-interval is iteratively narrowed down until the solution is reached. The bisection algorithm is necessary for the *lqr* since the *lqr* does not have a joint density associated. See Algorithm 1 in Appendix A for pseudo code.

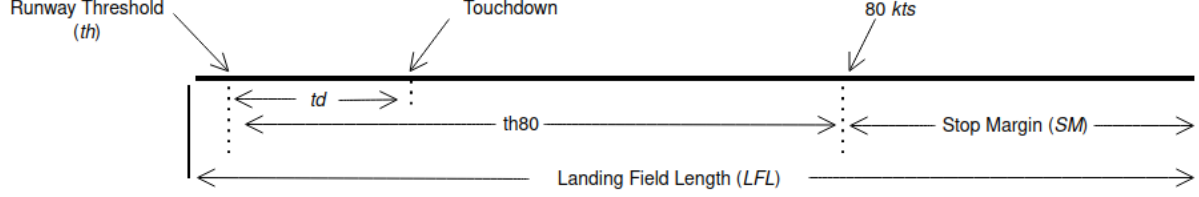
On the other hand, the Rosenblatt transform for D-vines is easily available for an observation and is implemented in the R-package **rvinecopulib** (Nagler and Vatter, 2021). The Rosenblatt transform will be utilized to compute the conditional distribution function at the chosen threshold c . For a random vector $\mathbf{V} = (V_1, \dots, V_p)^\top$ with joint distribution function F , let the conditional distribution function of V_j given V_1, \dots, V_{j-1} denoted by $F_{j|1, \dots, j-1}$, $j = 2, \dots, p$. Then, the random vector \mathbf{U} , where $U_1 := F(V_1)$ and $U_j := F_{j|1, \dots, j-1}(V_j | V_1, \dots, V_{j-1})$ for $j = 2, \dots, p$, is joint uniformly distributed. With the use of Equation (6), we can express $F_{j|1, \dots, j-1}(v_j | v_1, \dots, v_{j-1})$ for observed values $V_j = v_j, \dots, V_1 = v_1$, as $F_{Y|X_1, \dots, X_d}(c | x_1, \dots, x_d)$ for arbitrary values of c given the value $\mathbf{X} = \mathbf{x}$.

4 Data analysis

The critical event probabilities are estimated as in Equation (17) for the response *th80* given the contributing factors \mathbf{X} in Table 1. Mathematically, we write

$$\alpha_c(\mathbf{x}_i) = 1 - P(th80_i \leq c | \mathbf{X}_i = \mathbf{x}_i) \quad (18)$$

for $i = 1, \dots, 711$, and an appropriately chosen threshold c . The choice of c must be less than the Landing Field Length (*LFL*), leaving an appropriate *SM* distance for the aircraft to exit the runway or completely stop. Figure 5 illustrates a runway with *th80* as well as the distance from runway threshold to touchdown, denoted by (*td*). It is important to mention that we include *td* as a contributing factor. Next, more details are provided on the estimation of the associated D-vine regression model.

Figure 5: Runway with markings such as th , td , $th80$ and SM .

4.1 D-vine regression model estimation

Discussed in Section 3.4, we first estimate the marginal distribution functions of all variables parametrically or via a mixture of univariate normal distributions. Figure 12 in Appendix B displays, on the left, fitted univariate and a mixture of univariate normal density estimates on the original scale (raw data) for all variables and their respective histograms on the pseudo copula scale, PIT values, on the right of each sub-figure. In addition, Table 10 in Appendix B lists the univariate distribution family fitted for each variable. Some of the fitted parametric distributions consists of more than two parameters, *i.e.* the skew Student t, which is utilized for fitting $refAP$ and hws .

Following the fitted marginal distribution functions, we display in Figure 6 three different panels: the normalized contour plots on the lower diagonal, the PIT of the variables on the copula scale and the Kendall's tau dependence between the variables on the upper diagonal. The normalized contour plots represent the transformation of a bivariate copula density to a bivariate distribution with standard normal margins and density $g(z_1, z_2)$, where

$$g(z_1, z_2) = c(\Phi(z_1), \Phi(z_2)) \cdot \phi(z_1) \cdot \phi(z_2).$$

Here $\Phi(\cdot)$ and $\phi(\cdot)$ are the distribution and density of a standard normal distribution, respectively. Note that the dependence between $th80$ and lm is the strongest with an empirical $\hat{\tau}_{Kendall} = 0.46$, while hws is negatively dependent on $th80$ with $\hat{\tau}_{Kendall} = -0.25$. The pseudo copula data for each variable, which is derived from the fitted marginal distribution, is approximately uniform as seen by the diagonal panels of Figure 6. Among the 711 flights we are studying, we observe only 33 unique values for tsd . This is apparent in the pairwise scatter plots in which vertical and horizontal lines are visible in the upper diagonal panels of Figure 6. Further, the normalized contour plots on the lower diagonal panels assess departure from the Gaussian copula assumption if the contour lines are not elliptical. This is seen, for example, in the contour panel between $th80$ and the contributing factor lm .

We fit a D-vine copula based regression using the R package **vinereg** (Nagler, 2021). To allow for easy simulation, we utilize only parametric distributions for the pair copula families. Table 3 gives a summary of the estimated conditional quantile function:

$$\hat{q}_\alpha(hws, \dots, ea) = \hat{F}_{th80}^{-1} \left(\hat{C}_{V_{th80}|U_{hws}, \dots, U_{ea}}^{-1}(\alpha | \hat{u}_{hws}, \dots, \hat{u}_{ea}) \right), \quad (19)$$

where $th80$ is the response and the covariates (hws, \dots, ea) are the contributing factors listed in Table 1.

Table 3 Summary output of fitted D-vine quantile regression for the response variable $th80$ given the contributing factors. The summary table includes the following: fitted pair copula family $\hat{\mathcal{F}}_{1k_j; k_1, \dots, k_{j-1}}$, its parameters $\hat{\theta}_{1k_j; k_1, \dots, k_{j-1}}$, the estimated Kendall's tau $\hat{\tau}_{1k_j; k_1, \dots, k_{j-1}}$, the log-likelihood $ll_{1k_j; k_1, \dots, k_{j-1}}$, the $ll_{1k_j; k_1, \dots, k_{j-1}}^{aic}$, the $ll_{1k_j; k_1, \dots, k_{j-1}}^{bic}$ and a p_value.

name	k_j	k_1, \dots, k_{j-1}	$\hat{\mathcal{F}}_{1k_j; k_1, \dots, k_{j-1}}$	$\hat{\theta}_{1k_j; k_1, \dots, k_{j-1}}$	$\hat{\tau}_{1k_j; k_1, \dots, k_{j-1}}$	$ll_{1k_j; k_1, \dots, k_{j-1}}$	$ll_{1k_j; k_1, \dots, k_{j-1}}^{aic}$	$ll_{1k_j; k_1, \dots, k_{j-1}}^{bic}$	P-value
lm	7	-	bb8	3.62, 0.84	0.45	196.19	-388.37	-379.24	< 0.00
td	10	7	frank	4.43	0.42	151.77	-301.54	-296.97	< 0.00
hws	2	10, 7	gaussian	-0.50	-0.34	96.11	-190.22	-185.65	< 0.00
ea	11	2, 10, 7	gaussian	0.44	0.29	75.85	-149.70	-145.13	< 0.00
asd	5	11, 2, 10, 7	gaussian	0.45	0.30	81.00	-160.00	-155.43	< 0.00
temp	3	5, 11, 2, 10, 7	frank	1.86	0.20	34.87	-67.74	-63.18	< 0.00
tbs	8	3, 5, 11, 2, 10, 7	frank	2.11	0.22	42.56	-83.13	-78.56	< 0.00
bd	9	8, 3, 5, 11, 2, 10, 7	frank	2.02	0.22	36.25	-70.49	-65.93	< 0.00
trd	6	9, 8, 3, 5, 11, 2, 10, 7	gumbel	1.09	0.09	10.55	-19.11	-14.54	< 0.00
refAP	4	6, 9, 8, 3, 5, 11, 2, 10, 7	gumbel	1.12	-0.11	9.11	-16.22	-11.66	< 0.00

The variables are labeled with indices described in Table 4. Here k_1 denotes the first contributing factor added, and k_j , likewise, denotes the j^{th} contributing factor added in the D-vine. Table 3 includes the fitted pair copula family $\hat{\mathcal{F}}_{1k_j; k_1, \dots, k_{j-1}}$, its parameters $\hat{\theta}_{1k_j; k_1, \dots, k_{j-1}}$, the estimated Kendall's tau $\hat{\tau}_{1k_j; k_1, \dots, k_{j-1}}$, the log-likelihood



Figure 6: Dependence exploration for flight data (normalized contour plots on the lower diagonal panels, histograms of the *PIT* values on the diagonal panels and pairwise scatter plots of the *PIT* values with an associated empirical Kendall's τ value on the upper diagonal panels).

$ll_{1k_j; k_1, \dots, k_{j-1}}$, the $ll_{1k_j; k_1, \dots, k_{j-1}}^{aic}$ in Equation (15) and the $ll_{1k_j; k_1, \dots, k_{j-1}}^{bic}$ in Equation (16). It also includes the *p_value* of a likelihood ratio test. The test compares the D-vine regression model with k_1, \dots, k_{j-1} contributing factors to another one with an additional factor k_j using conditional log likelihoods.

We write the log likelihood for the pair copula term $c_{1k_j; k_1, \dots, k_{j-1}}$ as

$$ll_{1k_j; k_1, \dots, k_{j-1}} := \sum_{i=1}^n \ln(c_{1k_j; k_1, \dots, k_{j-1}}(C_{1|k_1, \dots, k_{j-1}}(\hat{u}_{i1} | \hat{u}_{ik_1}, \dots, \hat{u}_{ik_{j-1}}), C_{k_j|k_1, \dots, k_{j-1}}(\hat{u}_{ik_j} | \hat{u}_{ik_1}, \dots, \hat{u}_{ik_{j-1}}))).$$

Since the conditional log likelihood of the model $U_1|U_{k_1}, \dots, U_{k_j}$ is given by

$$c ll_{1|k_1, \dots, k_j} = \sum_{m=1}^j ll_{1k_m; k_1, \dots, k_{m-1}},$$

we have that the likelihood ratio test statistic is

$$2 \times [c ll_{1|k_1, \dots, k_j} - c ll_{1|k_1, \dots, k_{j-1}}] = 2 \times ll_{1k_j; k_1, \dots, k_{j-1}}.$$

If the corresponding $p_value < 0.05$, we have significant evidence that the additional contributing factor X_{k_j} is improving the model fit over the model with $X_{k_1}, \dots, X_{k_{j-1}}$ factors.

Table 4 Variable labels in the summary table of the estimated D -vine quantile regression.

Variable	<i>th80</i>	<i>hws</i>	<i>temp</i>	<i>refAP</i>	<i>asd</i>	<i>trd</i>	<i>lm</i>	<i>tbs</i>	<i>bd</i>	<i>td</i>	<i>ea</i>
Label	1	2	3	4	5	6	7	8	9	10	11

One of the contributing factors, *tsd*, was not selected as a candidate to maximize the *c ll*. The contributing factor *tsd* is also the variable with a few unique observations among the total 711 observations. For more details, Table 11 in Appendix B gives a full summary of the fitted D -vine copula.

4.2 *lqr* model estimation

Using the R package **quantreg** (Koenker, 2021), we fit a *lqr* model for the response variable, *th80*, conditioned on all contributing factors listed in Table 1. We write this as:

$$q_{\alpha}^{(l)}(hws, \dots, ea) := F_{th80|X}^{-1}(\alpha|hws, \dots, ea) \quad (20)$$

for different quantile levels $\alpha \in (0, 1)$. Table 5 gives a summary of the estimated *lqr* at two quantile levels: $\alpha = 0.5$ and $\alpha = 0.9$. The significance of the contributing factors on the response changes for different quantile levels. For instance, at $\alpha = 0.5$, the contributing factor *bd* has $p_value < 0.001$, whereas, at $\alpha = 0.9$, the p_value increases to more than 0.80. The method used to calculate standard error estimates is the bootstrap as proposed by Koenker and Hallock (2001).

Table 5 Two fitted *lqr* models at $\alpha = 0.5$ and $\alpha = 0.9$ with different significance of contributing factors.

Variable (quantile)	<i>th80</i> ($\alpha = 0.5$)			<i>th80</i> ($\alpha = 0.9$)		
	Value	Std. Error	p_value	Value	Std. Error	p_value
(Intercept)	362.91	512.81		-733.18	1,327.30	
hws	-32.13	3.91	***	-40.86	5.11	***
temp	4.01	0.74	***	3.27	1.18	***
refAP	-1.55	0.44	***	-0.29	1.31	
asd	27.59	3.54	***	38.22	5.28	***
trd	8.99	4.19	**	16.32	10.16	
tsd	14.21	14.55		13.95	29.66	
lm	3.95	0.42	***	5.86	0.47	***
tbs	25.47	5.25	***	10.02	3.59	***
bd	21.19	6.12	***	0.88	4.30	
td	1.01	0.03	***	0.89	0.08	***
ea	212.14	37.42	***	209.27	55.53	***
Observations	711					
Note: *p<0.1; **p<0.05; ***p<0.01						

Note that some estimates are not unique with respect to α . For example, it is possible to have two or more different quantile levels with the same estimate $\hat{q}_{\alpha}^{(l)}$ for one observation. Figure 7 displays two α values with the same conditional quantile estimate $\hat{q}_{\alpha}^{(l)} = 1460$ for flight 442. This illustrates the problem of quantile crossing, which occurs in our data.

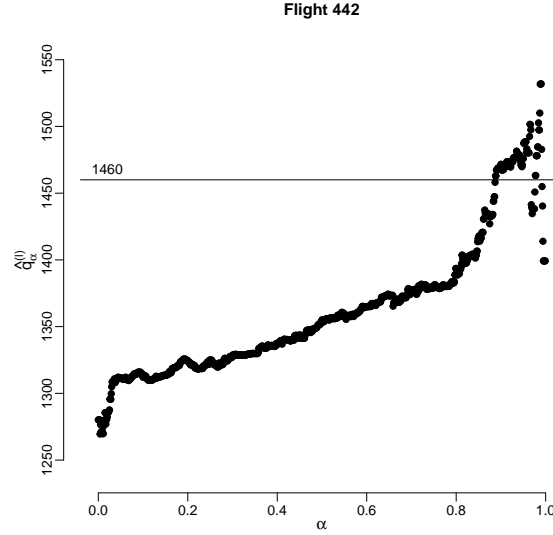


Figure 7: Non unique quantile levels, α , at the same threshold $c = 1460$ for flight 442.

4.3 Risky flight probability estimation

The number of flights having an estimate of $\alpha_c(\mathbf{x}_i)$ greater than 10^{-13} for $i = 1, \dots, 711$ is listed in Table 6 for three different thresholds c in meters, $c = (2200, 2400, 2500)^\top$. The estimated critical event probability, $\hat{\alpha}_c(\mathbf{x}_i)$, was obtained via the bisection algorithm for the estimated lqr of (20) and via the Rosenblatt transform of (19). The estimated lqr model uses all contributing factors for the probability estimation, no variable selection was performed. On the other hand, the estimated D-vine regression model uses ten of the contributing factors, leaving tsd out. The three different thresholds were chosen according to the landing field length described earlier in Section 2.

The estimated lqr model was not able to provide estimates greater than 10^{-13} beyond the observed maximum distance of $th80$ (2,606.77 m). The estimated D-vine regression model, however, provided nonzero estimates beyond the observed maximum distance of $th80$ for over 50% of the flights. For the D-vine approach, we further consider two cases where only Gaussian pair copula families are used (D-vine^{Gauss}) and several parametric pair copula families are used (D-vine^{Par}).

Table 6 Number of flights having estimates of $\alpha_c(\mathbf{x}_i)$ larger than 10^{-13} from three different models lqr , D-vine^{Gauss} and D-vine^{Par} for three different thresholds c in m .

	lqr (%)	D-vine ^{Gauss} (%)	D-vine ^{Par} (%)
2200 m	206 (28.97%)	709 (99.72%)	708 (99.58%)
2400 m	59 (8.30%)	709 (99.72%)	703 (98.87%)
2500 m	23 (3.23%)	706 (99.30%)	691 (97.19%)

Identification of risky flights

We investigate flights which have an estimated risk probability $\hat{\alpha}_c(\mathbf{x}_i) > 0.001$ and threshold $c = 2500 m$ for $i = 1, \dots, 711$. Among the 711 flights, we identify 41 such flights using the D-vine^{Par} approach. The largest risk probability estimate within this group is 0.202. In comparison to the other two approaches, the D-vine^{Gauss} identifies the least. Table 7 lists the five identified risky flights using the D-vine^{Gauss} approach, which are also among those identified in the lqr and the D-vine^{Par} approaches. The estimated risk probabilities from each approach are included in Table 7.

Because we are interested in studying the relationship between the contributing factors and the estimated risk probabilities for the risky flights, we will focus on the 41 flights identified using the D-vine^{Par} approach. The 41 estimated risk

Table 7 List of the five identified flights having an estimated risk probability $> 10^{-3}$ using the D-vine^{Gauss} approach compared to the other approaches with their respective probabilities.

flight	lqr_est_prb	D_vine_Gauss	D_vine_par
1	0.007	0.540	0.202
2	0.004	0.368	0.013
3	0.007	0.015	0.054
4	0.004	0.010	0.036
5	0.006	0.014	0.077

probabilities fall in the range $(0.001, 0.203)$, therefore, we transform the estimates to the real number line $(-\infty, \infty)$ using the logit function:

$$\eta_r = \text{logit}(\hat{\alpha}_c(\mathbf{x}_r)) = \ln \left(\frac{\hat{\alpha}_c(\mathbf{x}_r)}{1 - \hat{\alpha}_c(\mathbf{x}_r)} \right) \quad (21)$$

for $r = 1, \dots, 41$. Since, also, we want to compare the chosen contributing factors resulted from the D-vine^{Par} approach to each other in terms of how much impact they have on the estimated risk probability η_r , we standardize the factors X_{k_j} , $j = 1, \dots, 10$, using

$$z_{rk_j} := \frac{x_{rk_j} - \bar{x}_{k_j}}{\sqrt{\frac{\sum_{r=1}^{41} (x_{rk_j} - \bar{x}_{k_j})^2}{N-1}}}, \quad \text{with } \bar{x}_{k_j} = \frac{1}{41} \sum_{r=1}^{41} x_{rk_j}$$

for $r = 1, \dots, 41$. Figure 8 shows pairwise scatter plot matrices on the lower diagonal and pairwise empirical Kendall's τ on the upper diagonal. On the diagonal panels, we see density plots of the estimated risk probabilities on the logit scale and the contributing factors on the standardized scale. We add in blue fitted linear regression lines for each variable paired with another with 90% pointwise confidence intervals. For example, *hws* and *tbs* have a positive linear relationship shown by an upward pointing blue line in the scatter plot and an empirical Kendall's τ dependence equal to 0.37.

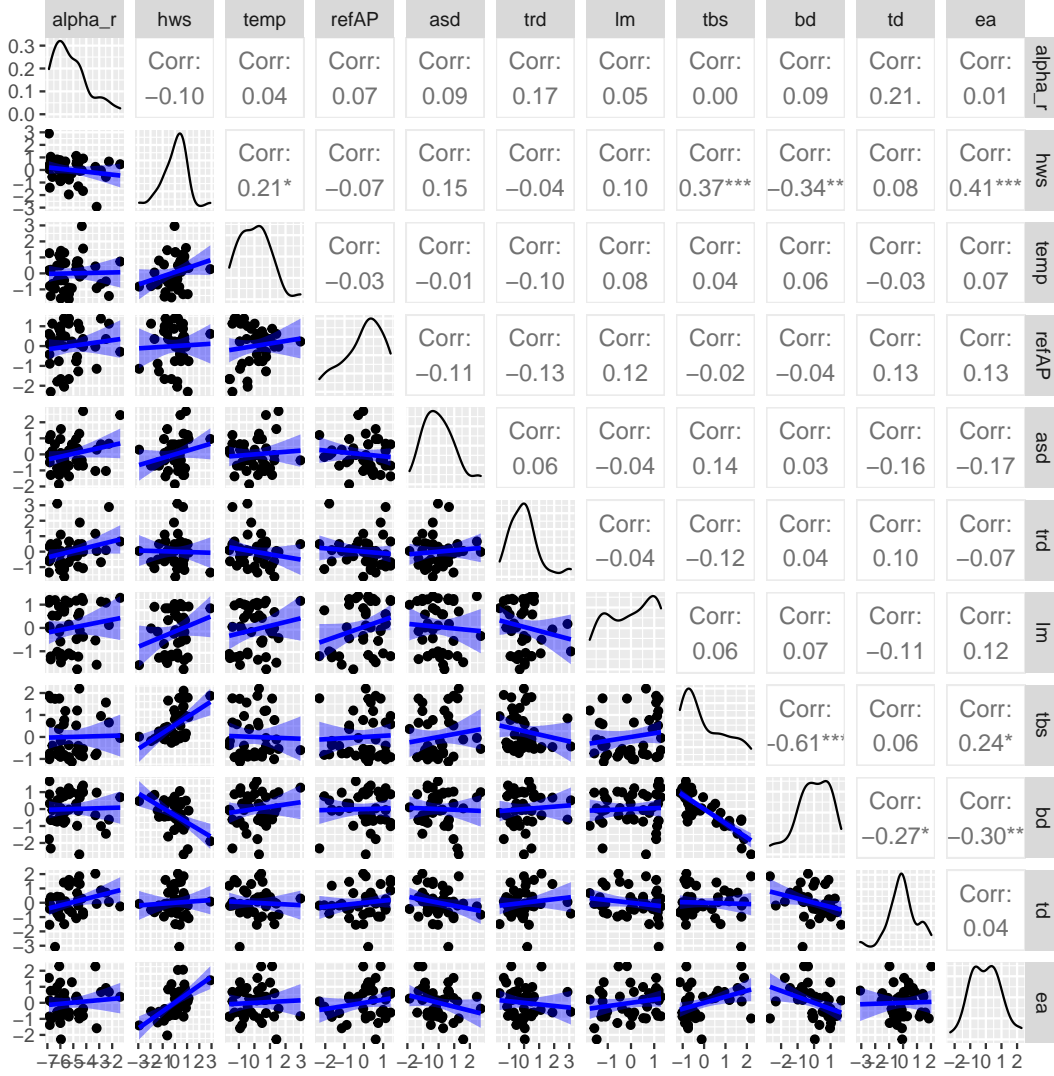


Figure 8: Pairwise scatter plots displayed on the lower diagonal panels, pairwise kendall's tau dependence on the upper diagonal and density plots of the variables on the diagonal panels.

Based on the scatter plots in Figure 8, we fit a multiple linear regression as the relationship between the estimated logit of risk probabilities and the standardized contributing factors could be explained linearly. We estimate the following multiple regression equation:

$$\alpha_c(\mathbf{x}_{rk_j}) = \beta_0 + \sum_{j=1}^{10} \beta_j z_{rk_j} + \epsilon_r, \quad (22)$$

where $\alpha_c(\mathbf{x}_{rk_j})$ denotes the estimated logit of the risk probability for flight r , $r = 1, \dots, 41$, and ϵ_r denotes normally distributed error with zero mean and σ^2 variance for flight r . Table 8 gives the estimated summary output of Equation (22). The output shows that a one standard deviation increase in hws leads to a -1.44 decrease in estimated logit of the risk probabilities. This estimated model gives an adjusted $R^2 = 0.80$, which states that 80% of the variability in the estimated logit of the risk probabilities is accounted for by the ten D-vine selected contributing factors. Figure 9 shows two types of box-plots for each contributing factor (red: risk and green: non-risk). The risk group corresponds to flights with an estimated risk probability $> 10^{-3}$, while the non-risk group corresponds to flights with an estimated risk probability $< 10^{-3}$. We note some contributing factors, *i.e.* hws , differ in their observed values for the two flight groups.

Table 8 Summary output of the estimated multiple linear regression in (22). The table includes estimated coefficients (Estimate), standard errors (Std. Error), t statistic values (t value) and p-values.

	Estimate	Std. Error	t value	Pr(> t)
(Intercept)	-5.20	0.10	-53.82	0.00
hws	-1.44	0.17	-8.62	0.00
ea	1.15	0.15	7.78	0.00
td	1.06	0.13	8.01	0.00
asd	1.02	0.12	8.33	0.00
tbs	0.96	0.24	3.97	0.00
bd	0.83	0.26	3.19	0.00
lm	0.47	0.12	4.02	0.00
trd	0.46	0.10	4.38	0.00
temp	0.28	0.11	2.48	0.02
refAP	-0.22	0.11	-1.97	0.06

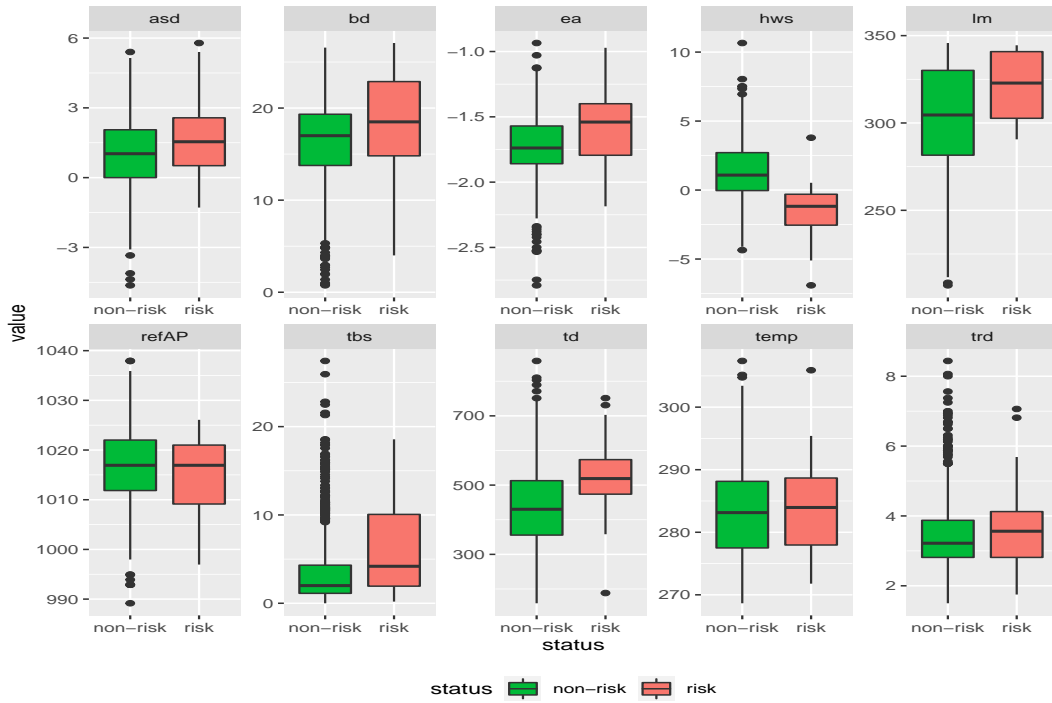


Figure 9: Box-plots of each contributing factor indicating the two different flight groups, red: risk and green: non-risk.

We rank the contributing factors based on their impact on the response variable measured by the size of the corresponding regression coefficient in Table 8. For the highest six contributing factors (*hws*, *ea*, *td*, *asd*, *tbs*, *bd*), we fit another multiple linear regression. The summary output, given in Table 9, gives an adjusted $R^2 = 0.60$, i.e. 60% of the variance in the estimated logit of the risk probabilities can be explained by these factors. In addition, we study the pairwise dependence between these contributing factors. Figure 10 displays similar panels to those in Figure 6 except that on the diagonal panels we fitted empirical distribution functions to the margins rather than univariate parametric distributions. We avoid parametric marginal distribution fitting due to the small sample size, $r = 41$. Among the lower diagonal panels, two panels show departure from the Gaussian copula assumption by the non elliptical shape of their contour lines. The contour panel between *hws* and *ea* shows a positive tail dependence, while the panel between *tbs* and *bd* shows a strong negative tail dependence.

Table 9 Summary output of a fitted multiple linear regression on a subset of the contributing factors.

	Estimate	Std. Error	t value	Pr(> t)
(Intercept)	-5.20	0.14	-38.42	0.00
bd	1.12	0.32	3.50	0.00
hws	-1.09	0.21	-5.24	0.00
tbs	1.07	0.31	3.46	0.00
td	1.05	0.18	5.95	0.00
ea	1.02	0.20	5.11	0.00
asd	0.96	0.17	5.75	0.00

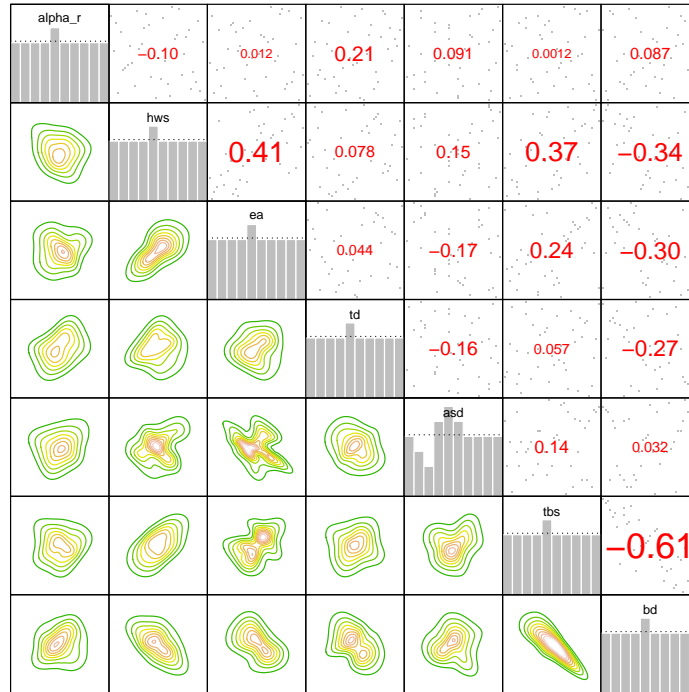


Figure 10: Dependence exploration for risky flights (normalized contour plots on the lower diagonal, histograms of the *PIT* values on the diagonal and pairwise scatter plots of the *PIT* values with associated empirical Kendall's τ values on the upper diagonal panels).

5 Discussion

We have shown that the probability of a flight decelerating to the controllable speed of 80 *kts* exceeding a chosen threshold c can be estimated conditioned on a set of influencing factors. The D-vine regression approach of Kraus and Czado (2017) was utilized since it is able to model very small conditional probabilities flexibly and estimate them analytically. In particular, we identified 41 flights, among 711, of the same aircraft type landed at the same airport having distance to controllable speed greater than 2500 meter with an estimated probability $> 10^{-3}$. The marginal effect of each contributing factor for these risky flights was further studied and ranked from the highest as follows: brake duration, headwind speed, time brake started, touchdown, equivalent acceleration and approach speed deviation. Also, the joint pairwise behavior among the contributing factors for the risky flights was investigated. We show that there is a non symmetric dependence between time brake started and brake duration as well as between headwind speed and equivalent acceleration.

Unlike the physics-based approach of Drees (2016) and Wang et al. (2020), the proposed D-vine approach does not require simulation nor subset simulation for small probabilities. Additionally, the D-vine approach does not require the discretization of the continuously measured factors and does not require experts' knowledge in network design as needed in Bayesian network approaches. Using the D-vine approach, also, nonzero probability estimates beyond the observed maximum distance of the controllable speed were provided in contrast to the classical *lqr* approach.

We have shown that our statistical approach is capable of quantifying the risk probability of runway overrun (the probability of a flight exceeding a chosen threshold at the controllable speed of 80 *kts*) and ranking the effects of the influencing factors on runway overrun. Similar scenarios, such as early landing and veer-offs, are also of a great importance in aviation safety and will be the focus of future investigations.

A Algorithms

A.1 Bisection Algorithm

The algorithm used to estimate (17) for the *lqr* in (1) is given the following:

Algorithm 1: Bisection algorithm for the *lqr*

```

for  $i = 1, \dots, n$  do
  Choose  $a$  and  $b \in (0, 1)$  with  $a < b$ .
  Evaluate  $\hat{q}_\alpha(x_1, \dots, x_d)$  in (1) for both  $\alpha = a$  and  $\alpha = b$ .
  if  $\hat{q}_c(x_1, \dots, x_d) \in (\hat{q}_a(x_1, \dots, x_d), \hat{q}_b(x_1, \dots, x_d))$  then
    1. Increase  $a$  by  $\delta$ ,  $\delta \in (0, 1)$ .
    2. Repeat.
  else
    if  $\hat{q}_c(x_1, \dots, x_d) \neq \hat{q}_a(x_1, \dots, x_d) \ \& \ \hat{q}_c(x_1, \dots, x_d) \neq \hat{q}_b(x_1, \dots, x_d)$  then
      1. Increase  $b$  by  $\delta$  and decrease  $a$  by  $\delta$ ,  $\delta \in (0, 1)$ .
      2. Repeat.
    else
      if  $\hat{q}_c(x_1, \dots, x_d) = \hat{q}_a(x_1, \dots, x_d) \ \& \ \hat{q}_c(x_1, \dots, x_d) \neq \hat{q}_b(x_1, \dots, x_d)$  then
        | Return  $a$ .
      else
        | Return  $b$ .
      end
    end
  end
end

```

B Figures and Tables

B.1 Pairwise Scatter Plots and Dependence

We display on the lower diagonal panels pairwise scatter plots, on the diagonal panels density plots and on the upper diagonal panels the empirical Kendall's τ . In the lower diagonal panels, we also add fitted linear regression lines in blue for each variable together with 90% confidence intervals.

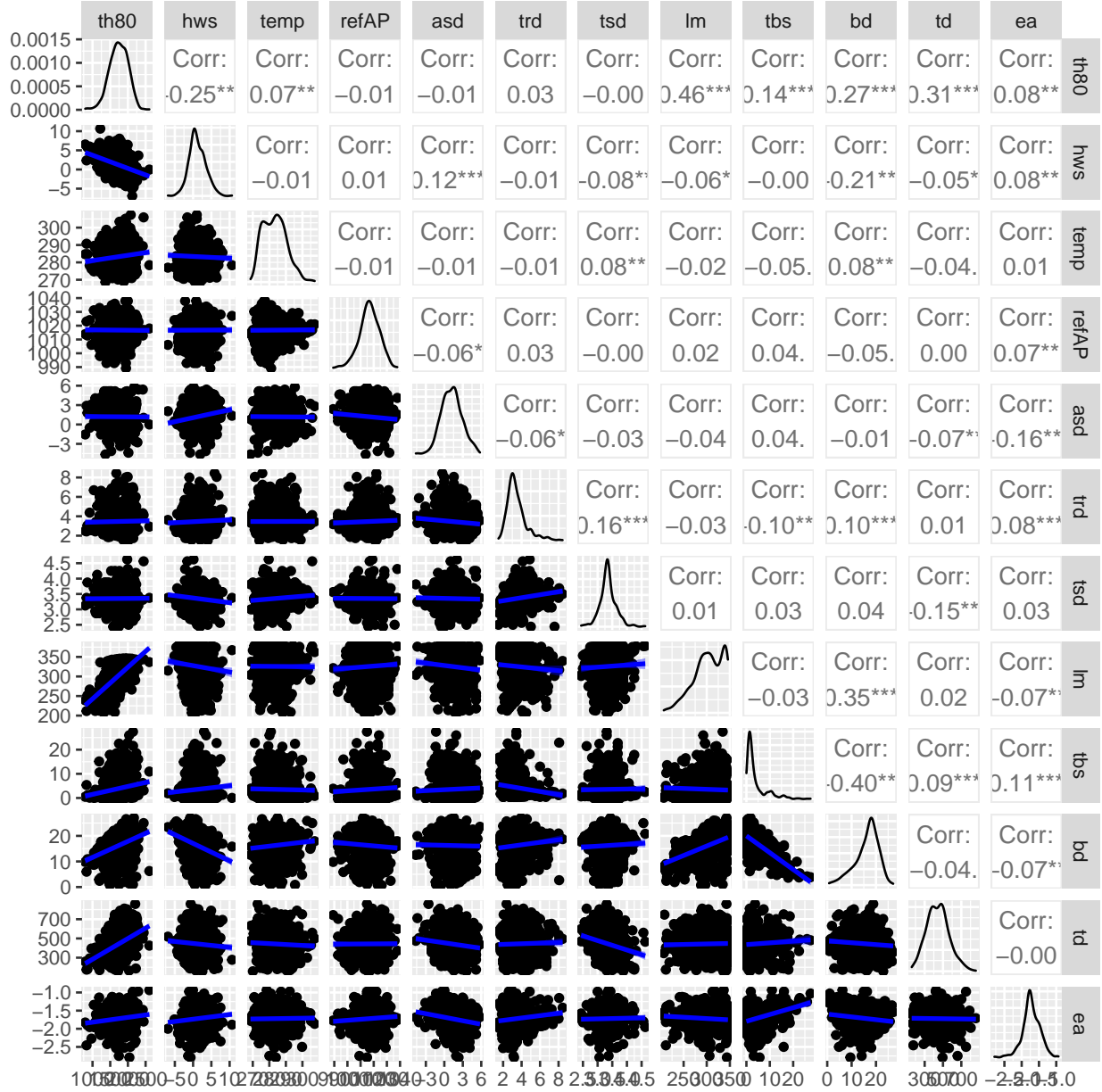


Figure 11

B.2 Fitted Marginal distribution functions

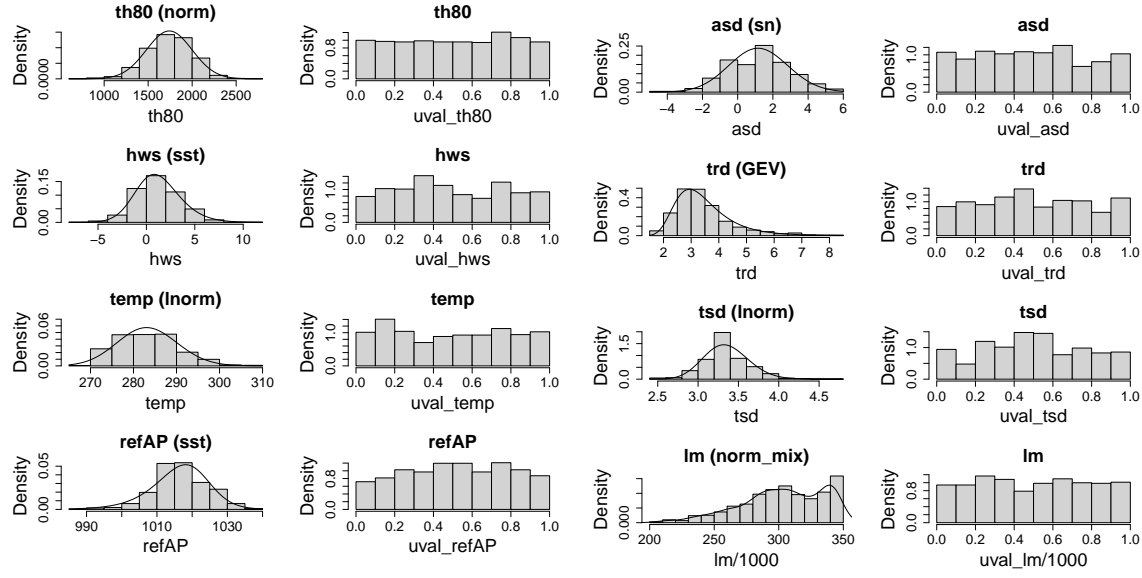
We list the fitted distribution families and their parameter estimates for all variables in our data set.

Table 10 Fitted marginal distributions for all variables and their parameter estimates.

Variable	Selected distribution	Parameter estimates (%)
th80	Normal	$[\hat{\mu}, \hat{\sigma}] = [1739.943, 259.2278]$
hws	Skew Student t.	$[\hat{\xi}, \hat{\omega}, \hat{\alpha}, \hat{\nu}] = [-0.7578, 2.9865, 1.4194, 19]$
temp	Log-Normal	$[\hat{\mu}, \hat{\sigma}] = [5.6462, 0.0245]$
refAP	Skew Student t.	$[\hat{\xi}, \hat{\omega}, \hat{\alpha}, \hat{\nu}] = [1023.067, 9.8146, -1.3456, 9]$
asd	Skew Normal	$[\hat{\xi}, \hat{\omega}, \hat{\alpha}] = [0.3789, 1.8669, 0.6545]$
trd	Generalized Extreme Value	$[\hat{\mu}, \hat{\sigma}, \hat{\nu}] = [2.9832, 0.7539, 0.0580]$
tsd	Log Normal	$[\hat{\mu}, \hat{\sigma}] = [1.2064, 0.0826]$
lm	Mixture of Normals	$[\hat{\mu}_1, \hat{\mu}_2, \hat{\mu}_3, \hat{\mu}_4] = [265.3788, 304.4632, 336.5114, 342.8597]$
		$[\hat{\sigma}_1, \hat{\sigma}_2, \hat{\sigma}_3, \hat{\sigma}_4] = [24.928, 16.6916, 4.0202, 1.4208]$
		$[\hat{\omega}_1, \hat{\omega}_2, \hat{\omega}_3, \hat{\omega}_4] = [0.2636, 0.4957, 0.1013, 0.1393]$
tbs	Generalized Extreme Value	$[\hat{\mu}, \hat{\sigma}, \hat{\nu}] = [1.6125, 1.5624, 0.5771]$
bd	Mixture of Normals	$[\hat{\mu}_1, \hat{\mu}_2] = [10.7978, 18.3855]$
		$[\hat{\sigma}_1, \hat{\sigma}_2] = [4.3706, 2.8982]$
		$[\hat{\omega}_1, \hat{\omega}_2] = [0.282, 0.7180]$
td	Gamma	$[\hat{\alpha}, \hat{\beta}] = [12.6204, 0.0285]$
ea	Skew Normal	$[\hat{\xi}, \hat{\omega}, \hat{\alpha}] = [-1.722, 0.2500, 0.9385]$

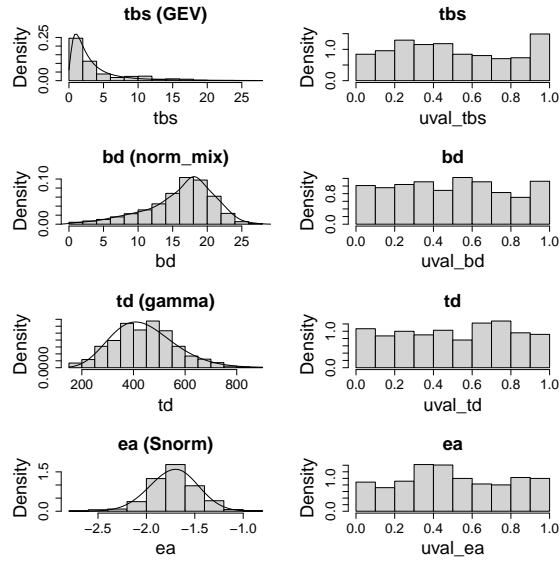
B.3 Histograms of Variables on the Original Scale and Pseudo Copula Scale

These histograms display the univariate and a mixture of univariate normal density estimates on the original scale as well as on the pseudo copula scale for all variables in our data.



(a) Density estimates and histograms for: *th80*, *hws*, *temp* & *refAP*.

(b) Density estimates and histograms for: *asd*, *trd*, *tsd* & *lm*.



(c) Density estimates and histograms for: *tbs*, *bd*, *td* & *ea*.

Figure 12: Density estimates on the original scale for all variables on the left of each sub figure and their corresponding histograms on the copula scale.

B.4 Fitted D-vine Copula

We give the full summary of the fitted D-vine copula, which consists of ten trees. The table includes entities such as the fitted pair copula family, its parameters, degrees of freedom (df), fitted Kendall's tau, the cll value as well as the upper and lower tail dependence coefficients (utd, ltd).

tree	conditioned	conditioning	family	rotation	parameters	df	tau	loglik	utd	ltd
1	1, 7		bb8	180	3.62, 0.84	2	0.45	196.19	0.00	0.00
1	7, 10		joe	180	1.03	1	0.02	1.16	0.00	0.04
1	10, 2		gaussian	0	-0.09	1	-0.06	2.70	0.00	0.00
1	2, 11		bb1	0	0.11, 1.03	2	0.07	6.48	0.04	0.00
1	11, 5		frank	0	-1.47	1	-0.16	18.96	0.00	0.00
1	5, 3		indep	0		0	0.00	0.00	0.00	0.00
1	3, 8		frank	0	-0.37	1	-0.04	1.44	0.00	0.00
1	8, 9		clayton	90	1.22	1	-0.38	175.76	0.00	0.00
1	9, 6		frank	0	0.90	1	0.10	7.58	0.00	0.00
1	6, 4		indep	0		0	0.00	0.00	0.00	0.00
2	1, 10	7	frank	0	4.43	1	0.42	151.77	0.00	0.00
2	7, 2	10	gaussian	0	-0.11	1	-0.07	3.79	0.00	0.00
2	10, 11	2	indep	0		0	0.00	0.00	0.00	0.00
2	2, 5	11	bb8	0	1.71, 0.80	2	0.14	18.92	0.00	0.00
2	11, 3	5	indep	0		0	0.00	0.00	0.00	0.00
2	5, 8	3	gumbel	0	1.05	1	0.05	2.31	0.06	0.00
2	3, 9	8	clayton	180	0.16	1	0.07	7.36	0.01	0.00
2	8, 6	9	gaussian	0	-0.09	1	-0.06	3.06	0.00	0.00
2	9, 4	6	clayton	270	0.13	1	-0.06	4.41	0.00	0.00
3	1, 2	10, 7	gaussian	0	-0.50	1	-0.34	96.11	0.00	0.00
3	7, 11	2, 10	bb8	270	1.25, 0.91	2	-0.08	5.87	0.00	0.00
3	10, 5	11, 2	clayton	90	0.15	1	-0.07	5.85	0.00	0.00
3	2, 3	5, 11	indep	0		0	0.00	0.00	0.00	0.00
3	11, 8	3, 5	joe	0	1.39	1	0.18	52.06	0.35	0.00
3	5, 9	8, 3	indep	0		0	0.00	0.00	0.00	0.00
3	3, 6	9, 8	indep	0		0	0.00	0.00	0.00	0.00
3	8, 4	6, 9	clayton	0	0.06	1	0.03	1.14	0.00	0.00
4	1, 11	2, 10, 7	gaussian	0	0.44	1	0.29	75.85	0.00	0.00
4	7, 5	11, 2, 10	clayton	270	0.11	1	-0.05	3.60	0.00	0.00
4	10, 3	5, 11, 2	frank	0	-0.35	1	-0.04	1.26	0.00	0.00
4	2, 8	3, 5, 11	indep	0		0	0.00	0.00	0.00	0.00
4	11, 9	8, 3, 5	t	0	0.09, 11.68	2	0.05	6.16	0.01	0.01
4	5, 6	9, 8, 3	clayton	270	0.09	1	-0.04	2.54	0.00	0.00
4	3, 4	6, 9, 8	joe	90	1.11	1	-0.06	3.45	0.00	0.00
5	1, 5	11, 2, 10, 7	gaussian	0	0.45	1	0.30	81.00	0.00	0.00
5	7, 3	5, 11, 2, 10	joe	270	1.10	1	-0.06	3.40	0.00	0.00
5	10, 8	3, 5, 11, 2	t	0	0.13, 9.10	2	0.09	8.99	0.02	0.02
5	2, 9	8, 3, 5, 11	gaussian	0	-0.43	1	-0.28	67.11	0.00	0.00
5	11, 6	9, 8, 3, 5	frank	0	1.16	1	0.13	10.76	0.00	0.00
5	5, 4	6, 9, 8, 3	frank	0	-0.55	1	-0.06	2.71	0.00	0.00
6	1, 3	5, 11, 2, 10, 7	frank	0	1.86	1	0.20	34.87	0.00	0.00
6	7, 8	3, 5, 11, 2, 10	joe	90	1.06	1	-0.03	1.53	0.00	0.00
6	10, 9	8, 3, 5, 11, 2	clayton	270	0.06	1	-0.03	1.34	0.00	0.00
6	2, 6	9, 8, 3, 5, 11	indep	0		0	0.00	0.00	0.00	0.00
6	11, 4	6, 9, 8, 3, 5	indep	0		0	0.00	0.00	0.00	0.00
7	1, 8	3, 5, 11, 2, 10, 7	frank	0	2.11	1	0.22	42.56	0.00	0.00
7	7, 9	8, 3, 5, 11, 2, 10	t	0	0.66, 6.52	2	0.46	205.66	0.25	0.25
7	10, 6	9, 8, 3, 5, 11, 2	clayton	180	0.06	1	0.03	1.31	0.00	0.00
7	2, 4	6, 9, 8, 3, 5, 11	indep	0		0	0.00	0.00	0.00	0.00
8	1, 9	8, 3, 5, 11, 2, 10, 7	frank	0	2.02	1	0.22	36.25	0.00	0.00
8	7, 6	9, 8, 3, 5, 11, 2, 10	gumbel	270	1.04	1	-0.04	3.37	0.00	0.00
8	10, 4	6, 9, 8, 3, 5, 11, 2	indep	0		0	0.00	0.00	0.00	0.00
9	1, 6	9, 8, 3, 5, 11, 2, 10, 7	gumbel	0	1.09	1	0.09	10.55	0.11	0.00
9	7, 4	6, 9, 8, 3, 5, 11, 2, 10	joe	180	1.20	1	0.10	9.25	0.00	0.22
10	1, 4	6, 9, 8, 3, 5, 11, 2, 10, 7	gumbel	90	1.12	1	-0.11	9.11	0.00	0.00

Table 11 D -vine tree sequence, tree T_1 to tree T_{10} , of 19. The variables (response and contributing factors) are labeled as in Table 4.

Acknowledgement

The authors would like to thank the CopFly team at the Institute of Flight System Dynamics of Prof. Dr.-Ing. Florian Holzapfel, Technical University of Munich, for their collaboration and insights. A special thanks goes to Xiaolong Wang for his immense help for explaining the data set used in this research.

Funding

The first author acknowledges the support of IGSSE, and the second author is supported by the German Research Foundation.

References

- Aas, K. (2016). Pair-copula constructions for financial applications: A review. *Econometrics*, 4(4):43.
- Aas, K., Czado, C., Frigessi, A., and Bakken, H. (2009). Pair-copula constructions of multiple dependence. *Insurance: Mathematics and Economics*, 44(2):182–198.
- Ahmed, M. M., Abdel-Aty, M., Lee, J., and Yu, R. (2014). Real-time assessment of fog-related crashes using airport weather data: A feasibility analysis. *Accident Analysis & Prevention*, 72:309–317.
- Anderson, J. (2007). *Fundamentals of Aerodynamics*. McGraw-Hill Series in Aeronautical and. McGraw-Hill Higher Education.
- Arnaldo Valdés, R. M., Gómez Comendador, V. F., Perez Sanz, L., and Rodriguez Sanz, A. (2018). Prediction of aircraft safety incidents using bayesian inference and hierarchical structures. *Safety Science*, 104:216–230.
- Au, S.-K. and Beck, J. L. (2001). Estimation of small failure probabilities in high dimensions by subset simulation. *Probabilistic Engineering Mechanics*, 16(4):263–277.
- Ayra, E. S., Ríos Insua, D., and Cano, J. (2019). Bayesian network for managing runway overruns in aviation safety. *Journal of Aerospace Information Systems*, 16(12):546–558.
- Bedford, T. and Cooke, R. (2001). Probability density decomposition for conditionally dependent random variables modeled by vines. *Annals of Mathematics and Artificial Intelligence*, 32(1):245–268.
- Bernard, C. and Czado, C. (2015). Conditional quantiles and tail dependence. *Journal of Multivariate Analysis*, 138:104–126.
- Burin, J. M. (2011). Keys to a safe arrival. <https://flightsafety.org/asw-article/keys-to-a-safe-arrival/>, Last accessed on 2022-02-25.
- ByesFusion (2020). Genie, graphical network interface.
- Chang, Y.-H., Yang, H.-H., and Hsiao, Y.-J. (2016). Human risk factors associated with pilots in runway excursions. *Accident Analysis & Prevention*, 94:227–237.
- Czado, C. (2010). Pair-copula constructions of multivariate copulas. In *Copula theory and its applications*, pages 93–109. Springer.
- Czado, C. (2019). *Analyzing Dependent Data with Vine Copulas: A Practical Guide With R*. Lecture Notes in Statistics. Springer International Publishing.
- Czado, C. and Nagler, T. (2022). Vine copula based modeling. *Annual Review of Statistics and Its Application*, 9(1):null.
- Drees, L. (2016). *Predictive Analysis: Quantifying Operational Airline Risks*. Dissertation, Technische Universität München, München.
- Drees, L., Wang, C., and Holzapfel, F. (2014). Using subset simulation to quantify stakeholder contribution to runway overrun. *Proceedings of Probabilistic Safety Assessment and Management PSAM*, 12.
- Flight Safety Foundation (2009). Reducing the risk of runway excursions.
- Gu, R.-p. and Wang, P. (2014). Estimation of wet and contaminated runway landing distance based on multiple linear regression. *Journal of Civil Aviation University of China*, 32(3):20.
- Hao, L. and Naiman, D. Q. (2007). *Quantile regression*. Number 149. Sage.
- Hu, C., Zhou, S.-H., Xie, Y., and Chang, W.-B. (2016). The study on hard landing prediction model with optimized parameter svm method. In *2016 35th Chinese Control Conference (CCC)*, pages 4283–4287. IEEE.

- IATA (2022). Air passenger numbers to recover in 2024. <https://www.iata.org/en/pressroom/2022-releases/2022-03-01-01/>, Last accessed on 2022-03-09.
- ICAO (2006). Icao annex 19, safety management. <https://www.icao.int/safety/SafetyManagement/>, Last accessed on 2022-02-25.
- ICAO (2013). *Safety Management Manual (SMS)*. Number Doc 9859. Third edition edition.
- Investigation, A. O. (2021). *Runway overrun involving Fokker 100, VH-NHY*.
- Jenkins, M. and Aaron, R. (2012). reducing runway landing overruns. *Aero Magazine*, 3:14–19.
- Joe, H. (1996). *Multivariate models and multivariate concepts*. Chapman & Hall.
- Joe, H. (2014). *Dependence modeling with copulas*. CRC press.
- Koenker, R. (2005). *Quantile Regression*. Econometric Society Monographs. Cambridge University Press.
- Koenker, R. (2021). *quantreg: Quantile Regression*. R package version 5.86.
- Koenker, R., Chernozhukov, V., He, X., and Peng, L. (2017). *Handbook of quantile regression*. CRC press.
- Koenker, R. and Hallock, K. F. (2001). Quantile regression. *Journal of economic perspectives*, 15(4):143–156.
- Koenker, R. W. and Bassett, G. (1978). Regression quantiles. *Econometrica*, 46(1):33–50.
- Kraus, D. and Czado, C. (2017). D-vine copula based quantile regression. *Computational Statistics & Data Analysis*, 110:1–18.
- Li, Q., Lin, J., and Racine, J. S. (2013). Optimal bandwidth selection for nonparametric conditional distribution and quantile functions. *Journal of Business & Economic Statistics*, 31(1):57–65.
- McLachlan, G. and Peel, D. (2000). *Finite Mixture Models*. Wiley Series in Probability and Statistics. Wiley.
- Nagler, T. (2021). *vinereg: D-Vine Quantile Regression*. R package version 0.7.4.
- Nagler, T. and Vatter, T. (2021). *rvinecopulib: High Performance Algorithms for Vine Copula Modeling*. R package version 0.5.5.1.1.
- Noh, H., Ghouch, A. E., and Van Keilegom, I. (2015). Semiparametric conditional quantile estimation through copula-based multivariate models. *Journal of Business & Economic Statistics*, 33(2):167–178.
- Patton, A. J. (2012). A review of copula models for economic time series. *Journal of Multivariate Analysis*, 110:4–18.
- Rosenblatt, M. (1952). Remarks on a multivariate transformation. *The Annals of Mathematical Statistics*, 23(3):470–472.
- Schöbi, R. and Sudret, B. (2019). Global sensitivity analysis in the context of imprecise probabilities (p-boxes) using sparse polynomial chaos expansions. *Reliability Engineering & System Safety*, 187:129–141.
- Scholz, D. (2012). *Aircraft design*. Springer.
- Sforza, P. (2014). *Commercial Airplane Design Principles*. Elsevier aerospace engineering series. Elsevier Science.
- Simons, M. (2015). *Model Aircraft Aerodynamics*. Chris Lloyd Sales & Marketing.
- Sklar, A. (1959). Fonctions de répartition à n dimensions et leurs marges. *Publications de l’Institut de Statistique de l’Université de Paris*, 8:229–231.
- Spokoiny, V., Wang, W., and Härdle, W. K. (2013). Local quantile regression. *Journal of Statistical Planning and Inference*, 143(7):1109–1129.
- Tang, X.-S., Li, D.-Q., Zhou, C.-B., and Phoon, K.-K. (2015). Copula-based approaches for evaluating slope reliability under incomplete probability information. *Structural Safety*, 52:90–99.
- Valdés, R. M. A., Comendador, F. G., Gordún, L. M., and Nieto, F. J. S. (2011). The development of probabilistic models to estimate accident risk (due to runway overrun and landing undershoot) applicable to the design and construction of runway safety areas. *Safety science*, 49(5):633–650.
- Wagner, D. C. and Barker, K. (2014). Statistical methods for modeling the risk of runway excursions. *Journal of Risk Research*, 17(7):885–901.
- Wang, C., Drees, L., Gissibl, N., Höndorf, L., Sembiring, J., and Holzapfel, F. (2014a). Quantification of incident probabilities using physical and statistical approaches. In *6th International Conference on Research in Air Transportation. Istanbul, Turkey*.
- Wang, L., Wu, C., and Sun, R. (2014b). An analysis of flight quick access recorder (qar) data and its applications in preventing landing incidents. *Reliability Engineering & System Safety*, 127:86–96.

- Wang, X., Fang, X., Beller, L., and Holzapfel, F. (2020). Calibration of contributing factors for model-based predictive analysis algorithm using polynomial chaos expansion methods.
- Wong, D. K., Pitfield, D., Caves, R. E., and Appleyard, A. (2006). Quantifying and characterising aviation accident risk factors. *Journal of Air Transport Management*, 12(6):352–357.
- You, X., Ji, M., and Han, H. (2013). The effects of risk perception and flight experience on airline pilots’ locus of control with regard to safety operation behaviors. *Accident Analysis & Prevention*, 57:131–139.
- Zhao, N. and Zhang, J. (2022). Research on the prediction of aircraft landing distance. *Mathematical Problems in Engineering*, 2022.
- Zwirgmaier, K. and Straub, D. (2016). A discretization procedure for rare events in bayesian networks. *Reliability Engineering & System Safety*, 153:96–109.